Available online at www.sciencedirect.com
SCIENCE DIRECT®
International Journal of Mass Spectrometry 241 (2005) 205–223
International Journal of Mass Spectrometry
www.elsevier.com/locate/ijms

Thermochemistry and structures of solvated S_N2 complexes and transition states in the gas phase: experiment and theory

B. Bogdanov, T.B. McMahon*

Department of Chemistry, University of Waterloo, Waterloo, Ont., Canada N2L 3G1

Received 16 November 2004; accepted 13 December 2004
Available online 8 January 2005

Dedicated to Professor Bill Hase on the occasion of his 60th birthday.

Abstract

The standard enthalpy and entropy changes (ΔH° and ΔS°) for the formation of solvated S_N2 complexes (S)X^-(RY) (X, Y = Cl, Br; R = $(CH_3)_2CH$; S = CH_3OH, CH_3CN, $(CH_3)_2CO$, CH_3CF_2H) have been determined by pulsed-ionization high pressure mass spectrometry. Not surprisingly, solvent effects are evident even at this mono-salvation level. Structures of solvated S_N2 complexes and transition states for the $Cl^-(S) + CH_3Cl$ S_N2 reaction (S = H_2O, H_2S, NH_3, PH_3, SO_2) have also been determined at the MP2/6-31+G(d) level of theory. A large variety of solvent dependent structures have been obtained, showing solvent reorganization upon going from the complex to the transition state. Standard binding and activation enthalpies (ΔH°_{298} and $\Delta H^\ddagger_{298}$) were determined at the MP2/6-311+G(3df,2p)//MP2/6-31+G(d,p) level of theory. For the $Cl^-(H_2O) + CH_3Br$ and $Br^-(H_2O) + CH_3Cl$ reactions, structures and enthalpies were calculated at the MP2/[6-31+G(d)/LanL2DZ(spd)] and MP2/[6-311+G(3df,2p)/LanL2DZ(spdf)]//MP2/[6-31+G(d)/LanL2DZ(spd)] level of theory. For the $Cl^- + CH_3Br$ and $Cl^-(H_2O) + CH_3Br$ reactions potential energy surface scans were performed at the MP2/[6-31+G(d)/LanL2DZ(spd)] level of theory. Formation of the two possible sets of solvated products, $Br^-(H_2O) + CH_3Cl$ and $Br^- + (CH_3Cl)(H_2O)$ proceeds through two different surfaces. Water transfer to the leaving group can be facilitated by rotation of the $Br^-(CH_3Cl)$ part in the exit channel $Br^-(CH_3Cl)(H_2O)$ complex. Finally, for the $Cl^- + CH_3Cl$ reactions in the condensed phase, complexation and activation energies ($\Delta E(\varepsilon)$ and $\Delta E^\ddagger(\varepsilon)$) were determined for a variety of solvents at the MP2/6-31+G(d) level of theory using the isodensity polarized continuum model. A linear correlation between $-\Delta E(\varepsilon)$ and $\Delta E^\ddagger(\varepsilon)$ was obtained, and a similar correlation exists for the mono-solvated gas phase S_N2 reaction, indicating that mono-solvation already exhibits some features of the condensed phase reaction.

Keywords: S_N2 reaction; Potential energy surfaces; Thermochemistry; Structure; Transition states

1. Introduction

Bimolecular nucleophilic displacement (S_N2) reactions in the condensed phase are among the most important reactions in chemistry (Eq. (1)), and have been studied from the 1930's onward, initially by Ingold [1], and followed by many others [2–10].

$$X^- + RY \rightarrow XR + Y^- \quad (1)$$

The acronym S_N2 comes from the fact that the rates of such reactions were found to be first order in both the nucleophile and substrate concentrations, $[X^-]$ and [RY], respectively (Eq. (2), making the overall reaction second order.

$$\text{rate} = k[X^-][RY] \quad (2)$$

In Fig. 1 schematic potential energy profiles for four hypothetical condensed phase and gas phase S_N2 reactions are shown. For all four situations the transition state corresponds to a penta-coordinated complex, $[XRY]^{-\ddagger}$. The increase in the barrier height on going from the gas phase to the condensed phase is mainly due to the differential solvation of

* Corresponding author. Tel.: +1 519 888 4591; fax: +1 519 746 0435.
E-mail address: mcmahon@uwaterloo.ca (T.B. McMahon).

1387-3806/$ – see front matter © 2004 Elsevier B.V. All rights reserved.
doi:10.1016/j.ijms.2004.12.018

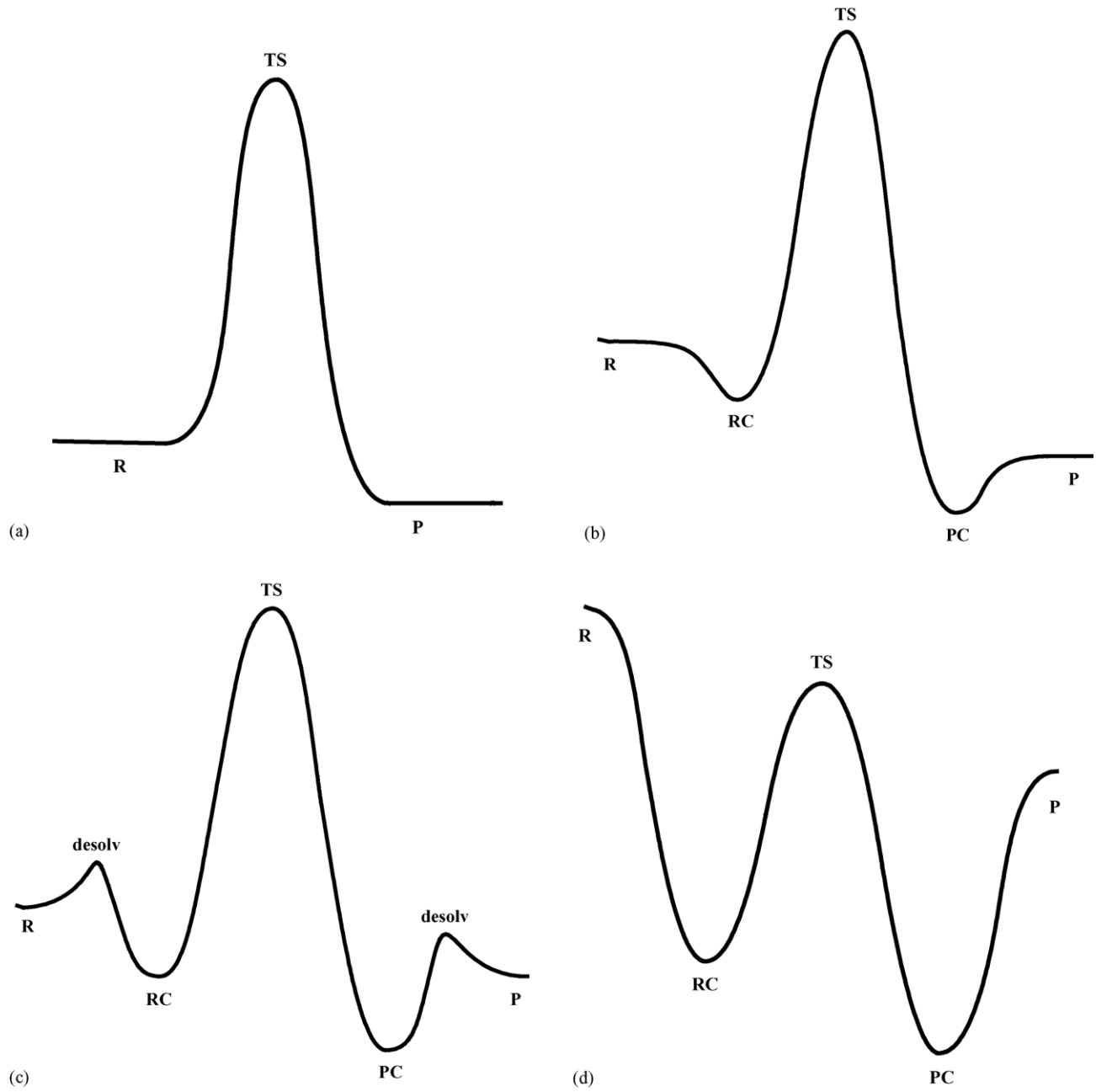

Fig. 1. (a) Condensed phase unimodal reaction energy profile (R = reactants, TS = transition state, P = products); (b) condensed phase double-well reaction energy profile for weak solvation (RC = reactants complex, PC = products complex); (c) condensed phase double-well reaction energy profile for strong and asynchronous desolvation and ion–molecule complexation (desolv = desolvation) and (d) gas phase double-well reaction energy profile.

the reactants and the transition state. This is caused by the greater extent of delocalization of charge in the transition state as opposed to the significantly more localized charge situation in the isolated nucleophile. A large variety of barrier heights have been determined, and these are very much solvent dependent [1–6,9]. Unfortunately, the extent of solvation of the nucleophile and transition state for various solvents may be different, and in addition the solvation of the substrate must also be considered [5,6]. The effects of counter ions and competitive reactions may also play a role and these should also be accounted for. In the condensed phase, S_N1 and E2 reactions may compete with S_N2 reactions, and the extent to which this occurs is very sensitive to the nature of the alkyl group, R.

In order to bridge the gap between the gas and condensed phases, studies of prototype micro-solvated S_N2 species have been performed in the gas phase (Eq. (3)) using a variety of experimental techniques [11–26]. By performing these kinds of experiments it is hoped to gain additional insight into the intrinsic contribution of the solvent molecules to the progress

Table 1
Overview of published work on solvated S_N2 reactions in the gas phase

$X^-(S)_n$	RY	n	Method	Quantity	Reference
$OH^-(H_2O)_n$	CH_3Br	0–3	FA	$k_{300\,K}$	[11]
$OH^-(H_2O)_n$	CH_3Br	1	SIFT	$k_{300\,K}$	[12]
$OH^-(H_2O)_n$	CH_3Cl	0–2	Bq	$\sigma(E_T)$	[13]
$RO^-(ROH)_n$	CH_3Cl	0–3	FA	$k_{295\,K}$	[14]
$RO^-(ROH)_n$	CH_3Br	0–3	FA	$k_{295\,K}$	[14]
$F^-(ROH)_n$	CH_3Cl	0–3	FA	$k_{295\,K}$	[15]
$F^-(ROH)_n$	CH_3Br	0–3	FA	$k_{295\,K}$	[15]
$Cl^-(ROH)_n$	CH_3Br	0–3	FA	$k_{295\,K}$	[15]
$OD^-(D_2O)_n$	CH_3Cl	0–2	VT-SIFT	$k_{200–500\,K}$	[16]
$OH^-(H_2O)_n$	CH_3CN	1	VT-SIFT	$k_{240–363\,K}$	[17]
$OH^-(H_2O)_n$	CH_3CN	0–2	SIFT	$k_{298\,K}$	[17]
$Cl^-(CHCl_3)_n$	CH_3Br/CH_3I	0–2	KIMMS	$k_{398\,K}$	[19]
$F^-(H_2O/D_2O)_n$	CH_3X/CD_3X	0,1	FA-SIFT	$k_{302\,K}$, k_H/k_D	[20]
$OH^-(H_2O)_n$	CH_3Cl	0–2	Bq	$\sigma(E_T)$	[21]
$OH^-(H_2O)_n$	CH_3Br	0,1	Bq	$\sigma(E_T)$	[21]
$OH^-(H_2O)_n$	CH_3Br	0–4	VT-SIFT	k_T	[22]
$F^-(H_2O)_n$	CH_3Br	0–5	VT-SIFT	k_T	[24]
$Cl^-(H_2O)_n$	CH_3Br	1–3	VT-SIFT	k_T	[25]

of these reactions.

$$X^-(S)_n + RY \rightarrow Y^-(S)_m + RX + (n-m)S \quad (3)$$

In Table 1 an overview is given of those systems that have been investigated experimentally to date in the gas phase. As can be seen, the main focus has been on obtaining kinetic data, although isotope effects, cross sections, and product ion distributions were also studied and reported. The main conclusion of this body of work has been that dramatic changes in reactivity can be observed, even with the addition of a single solvent molecule. Further, most reactions become too slow for their rate constants to be measurable with the addition of two or more solvent molecules. With respect to the product ion distributions some interesting results have also been reported. For most mono-solvated reactions only a small fraction of the leaving groups are solvated (Eq. (4)) [11–16,19–22,24,25], even though this reaction pathway is more exothermic than formation of the non-solvated leaving group (Eq. (5)).

$$X^-(S) + RY \rightarrow Y^-(S) + RX \quad (4)$$

$$X^-(S) + RY \rightarrow Y^- + RX + S \quad (5)$$

For more extensively solvated nucleophiles ($n \geq 2$), complex formation (Eq. (6)) and ligand-switching (Eq. (7)) become more important [24,25].

$$X^-(S)_n + RY + M \rightarrow (S)_n X^-(RY) + M \quad (6)$$

$$X^-(S)_n + RY \rightarrow (S)_{n-1} X^-(RY) + S \quad (7)$$

Craig and Brauman [23,26] showed that introduction of an ω-substituent (X = CN, Cl, OH) onto a primary *n*-alkyl chloride significantly enhanced the rate of gas phase S_N2 identity chloride displacement reactions (Eq. (8)).

$$Cl^- + {}^*Cl(CH_2)_n X \rightarrow {}^*Cl^- + Cl(CH_2)_n X \quad (8)$$

This was the result of intramolecular micro-solvation of the S_N2 transition state, facilitated by the presence of the remote functional group and the consequent through-space ion–dipole stabilization interactions.

As can be seen from Table 1, most solvated nucleophiles studied to date involve water or other strongly bound protic solvents. However, in actual condensed phase work, it has been known that S_N2 reactions proceed much faster in polar, aprotic solvents [5,6]. Similar trends can be observed for the growing, but still relatively small number of published theoretical studies on solvated S_N2 reactions. Morokuma [27] showed that for Eq. (9) ($n = 1, 2$) solvent transfer can take place before, after, and during the Walden inversion of the methyl group.

$$Cl^-(H_2O)_n + CH_3Cl \rightarrow Cl^-(H_2O)_n + CH_3Cl \quad (9)$$

Hu and Truhlar [28] have calculated transition state theory rate constants and kinetic isotope effects at the MP2/aug-cc-pVDZ level of theory for Eqs. (10) and (11), and found excellent agreement with the experimental data from O'Hair et al. [20].

$$F^-(H_2O) + CH_3Cl \rightarrow Cl^-(H_2O) + CH_3F \quad (10)$$

$$F^-(H_2O) + CH_3Cl \rightarrow Cl^- + CH_3F + H_2O \quad (11)$$

In addition, the energy of the solvated transition state, $[(H_2O)FCH_3Cl]^{-\ddagger}$, was calculated to be -2.2 kcal mol^{-1} with respect to the reactants. Bickelhaupt et al. investigated the effect of solvation by one to four HF molecules on the E2 and S_N2 reaction of F^- and C_2H_5F [29]. The main observation was the increased importance of the S_N2 over the E2 pathway as the number of solvent molecules increased. Recently, several very interesting articles have been published that reported results on ab initio molecular dynamics simulations of solvated S_N2 reactions. Tachikawa showed that the reaction between $F^-(H_2O)$ and CH_3Cl can proceed via three

pathways (Eqs. (12)–(14)), and that the branching ratios are dependent on the centre-of-mass collision energy [30,31].

$$F^-(H_2O) + CH_3Cl \rightarrow Cl^- + CH_3F + H_2O \quad (12)$$

$$F^-(H_2O) + CH_3Cl \rightarrow Cl^-(H_2O) + CH_3F \quad (13)$$

$$F^-(H_2O) + CH_3Cl \rightarrow Cl^- + (CH_3F)(H_2O) \quad (14)$$

At a collision energy of 10.0 kcal mol^{-1}, the branching ratios are 0.55:0.04:0.41, while at 17.7 and 25.0 kcal mol^{-1} they are 0.46:0.18:0.36 and 0.35:0.43:0.22, respectively [31]. These results thus clearly show that solvent transfer can be increased with increased kinetic energy which evidently aids in passage over a barrier. It was also shown that solvent transfer only takes place in a very narrow range of the HO–H$\cdots$F$^-\cdots$CH$_3$Cl angles, thereby explaining why solvent transfer in these reactions has been observed so seldom in experiments. Finally, Raugei et al. [32] have reported data on the potential energy profiles and stationary points for Eq. (15) (n = 0–2).

$$Cl^-(H_2O)_n + CH_3Br \rightarrow \text{products} \quad (15)$$

By molecular dynamics (MD) computations these authors were able to confirm reports by Seeley et al. [25] on similar reactions. They observed for ligand switching for both n = 1 and 2. In addition, for the n = 1 S_N2 reaction an activation energy of 2.5 kcal mol^{-1} was measured, while at the B3LYP/6-311+G(d,p) level of theory a value of −1.9 kcal mol^{-1} was found. Mohamed and Jensen carried out DFT and ab initio computations at the B3LYP/6-31+G(d) and MP2/6-31+G(d)//B3LYP/6-31+G(d) levels of theory for the micro-solvated reactions, Eq. (16),

$$Cl^-(S)_n + RCl \rightarrow ClR + Cl^-(S)_n \quad (16)$$

with R = CH$_3$, CH$_3$CH$_2$, (CH$_3$)$_2$CH, (CH$_3$)$_3$C; S = H$_2$O, CH$_3$OH, CH$_3$CN, (CH$_3$)$_2$CO, (CH$_3$)$_2$O, CH$_3$CH$_2$CH$_3$, n = 0–2, 0–4 (S = H$_2$O only) [33]. In addition, to include effects of bulk solvation, the reactions were also studied using the polarizable continuum model (PCM) at the B3LYP/6-31+G(d) level of theory. Not surprisingly, it was found that for all solvents used the barrier heights increase with the number of solvent molecules and that, except for R = (CH$_3$)$_3$C, the transition state structures do not change substantively upon solvation. The PCM model has been shown to underestimate the trend in increase of activation energies relative to the gas phase, which depends on the dielectric constant of the solvent. Finally it should be noted that other studies of solvated S_N2 reactions have been reported, but their main focus has been on equilibrium and non-equilibrium solvent effects, and kinetic solvent isotope effects [34–39]. These topics, while interesting and important, will not be discussed, within the context of the present work.

As can be seen in Fig. 1b and c and from Eq. (6), the solvated S_N2 complexes, $(S)_nX^-(RY)$, are intermediates on the potential energy surfaces of S_N2 reactions in the condensed phase and in micro-solvated gas phase reactions. Surprisingly, no experimental thermochemical data on important cluster ions of this type have been reported to date. As noted above, most computational data on solvated S_N2 reactions have involved water as the solvent and, it would seem logical to extend such investigations to more commonly employed solvent types as well.

In the present work, a combined PHPMS and computational ab initio study is presented to add information on the thermochemistry and structures of solvated S_N2 complexes and transition states. Various solvents have been investigated to gain insight into the intrinsic nature of solvent effects at the micro-solvation level. Some of the solvents studied, both in the experiments and the computations, are not necessarily commonly employed but they do serve as useful models for various solvent types.

2. Experimental

All measurements were carried out on a pulsed-ionization high pressure mass spectrometer (PHPMS), configured around a VG 8-80 mass analyzer. The instrument, constructed at the University of Waterloo, has been described in detail previously [40].

Gas mixtures were prepared in a 5 L heated stainless steel reservoir at 350–380 K, by using CH_4 as the bath gas at a pressure of 300–800 Torr. Chloride ion was generated from trace amounts of CCl_4 by dissociative electron capture of thermalized electrons from 50 to 500 μs pulses of a 2 keV electron gun beam. Two different methods were used to generate bromide ion. In the first, bromide ion was generated from CBr_4 by dissociative electron capture, in analogous fashion to the generation of chloride ion, by injecting 3 μl of a CBr_4/C_6H_6 solution, with a CBr_4 concentration of 0.287 M, into the reservoir. The second method, which generates bromide ion more efficiently, involves the S_N2 reaction between Cl^- and n-butyl bromide (Eq. (17)).

$$Cl^- + CH_3CH_2CH_2CH_2Br \rightarrow Br^- + CH_3CH_2CH_2CH_2Cl \quad (17)$$

The two alkyl halides ((CH$_3$)$_2$CHCl and (CH$_3$)$_2$CHBr) and the four solvents (CH$_3$OH, CH$_3$CN, (CH$_3$)$_2$CO, and CH$_3$CF$_2$H) were added in a wide variety of relative amounts, depending upon the ion source temperature and the nature of the experiment involved. The ion source pressure and temperature ranged from 4.0 to 7.5 Torr and 300 to 380 K, respectively.

Time intensity profiles of mass selected ions were monitored by using a PC based multi-channel scalar (MCS) data acquisition system, configured at 50–200 μs dwell time per channel over 250 channels. Additive accumulations of ion signals from 1000 to 2000 electron gun beam pulses were used.

Equilibrium constants (K_{eq}) at different absolute temperatures for the various halide ion–solvent (Eq. (18)), solvated

S_N2 (Eq. (19)), and S_N2 complex solvation (Eq. (20)) clustering equilibria were determined from Eqs. (21)–(23), respectively.

$$X^- + S \rightleftharpoons X^-(S) \quad (18)$$

$$X^-(S) + RY \rightleftharpoons (S)X^-(RY) \quad (19)$$

$$X^-(RY) + S \rightleftharpoons (S)X^-(RY) \quad (20)$$

$$K_{eq,18} = \frac{\mathrm{Int}(X^-(S))}{\mathrm{Int}(X^-)} \cdot \frac{P^o}{P_{S,source}} \quad (21)$$

$$K_{eq,19} = \frac{\mathrm{Int}((S)X^-(RY))}{\mathrm{Int}(X^-(S))} \cdot \frac{P^o}{P_{RY,source}} \quad (22)$$

$$K_{eq,20} = \frac{\mathrm{Int}((S)X^-(RY))}{\mathrm{Int}(X^-(RY))} \cdot \frac{P^o}{P_{S,source}} \quad (23)$$

In Eqs. (21)–(23) $\mathrm{Int}(X^-(S))/\mathrm{Int}(X^-)$, $\mathrm{Int}((S)X^-(RY))/\mathrm{Int}(X^-(S))$, and $\mathrm{Int}((S)X^-(RY))/\mathrm{Int}(X^-(RY))$ are the ion intensity ratios of the $X^-(S)$ and X^-, $(S)X^-(RY)$ and $X^-(S)$, and $(S)X^-(RY)$ and $X^-(RY)$ ions at equilibrium, respectively; P^o is the standard pressure (1 atm), and $P_{S,source}$, and $P_{RY,source}$ are the partial pressures (in atm) of the solvent (S) and the S_N2 substrate (RY) in the ion source, respectively.

From the equilibrium constants the standard Gibbs' free energy changes (ΔG°) at different absolute temperatures (T) can be calculated from Eq. (24).

$$\Delta G^\circ = -RT \ln(K_{eq}) \quad (24)$$

By combining Eqs. (24) and (25) the van't Hoff equation, Eq. (26), can be obtained.

$$\Delta G^\circ = \Delta H^\circ - T\Delta S^\circ \quad (25)$$

$$\ln(K_{eq}) = \frac{\Delta S^\circ}{R} - \frac{\Delta H^\circ}{R}\frac{1}{T} \quad (26)$$

By plotting $\ln(K_{eq})$ versus $1/T$, ΔH° and ΔS° can be obtained directly from the slope and the intercept, respectively. While both ΔH° and ΔS° values may have a temperature dependence the application of the van't Hoff equation implies that they are constant throughout the temperature range examined (21–112 °C). Moreover, our analysis of our experimental data for many different types of association equilibria, with the aid of ab initio calculations, has revealed that even though individual ΔH_f and S_f may be strongly temperature dependent, the association reaction ΔH° and ΔS° are not and thus the reported experimental data will, within the experimental error, reflect the corresponding ΔH°_{298} and ΔS°_{298} values. Hence comparison of the experimental data with ab initio calculated ΔH°_{298} and ΔS°_{298} is expected to be valid. Relative experimental errors reported are the result of the precision of the equilibrium constant measurements obtained through regression analysis while the somewhat larger absolute experimental errors contain contributions from estimated uncertainties in temperature and pressure measurements.

Equilibrium constants were calculated from the experimental data for various isotope pairs. For example, the ratios $^{35}Cl^-(S)/(S)^{35}Cl^-(R^{35}Cl)$ and $^{35}Cl^-(S)/(S)^{35}Cl^-(R^{37}Cl)$, and $^{35}Cl^-(S)/(S)^{35}Cl^-(R^{79}Br)$ and $^{35}Cl^-(S)/(S)^{35}Cl^-(R^{81}Br)$ would be measured and then these data were statistically corrected using the appropriate isotopic composition of the ions and neutral molecules involved in the equilibrium.

Carbon tetrabromide, *iso*-propyl bromide and chloride, *n*-butyl bromide, and 1,1-difluoroethane were obtained from Aldrich Chemical Company Inc., acetonitrile and benzene from BDH, acetone and methanol from Fisher Scientific, carbon tetrachloride from J.T. Baker Chemical Co., and methane from Praxair. All chemicals were used as received

3. Computational

All computations were performed using the Gaussian 98 and 98W suites of programs [41]. Geometries were optimized using the HF [42] and MP2(fc) [43] methods in combination with the 6-31+G(d,p) (**a**) [44–48] basis set. Normal mode vibrational frequencies were calculated at the HF level of theory, scaled by 0.8930 [49–51], while for some systems the MP2 level of theory was used, scaled by 0.90 [49]. Single point energy computations were performed at the MP2(fc) level of theory in combination with the 6-311+G(3df,2p) (**b**) [45–48,52] basis set, using the MP2/**a** geometry. For the systems containing bromine and iodine, similar computations were performed, except that the 6-31+G(d) (**c**) [44–48,53] basis set was used for H, C, N, O, and Cl, while for Br and I a modified LanL2DZ ECP basis set, here indicated as LanL2DZ(spd) (**d**) [54,55], was used. The normal mode vibrational frequencies were scaled by 0.8970 [49]. For the single point energy computations for bromine and iodine, the LanL2DZ(spd) basis set was used, including an extra f function, indicated as LanL2DZ(spdf) (**e**) [54,55]. For some of the systems investigated, computations were also performed at the G2(MP2) level of theory [56] to further test the suitability of the above mentioned method on the systems of interest. For the $Cl^- + CH_3Br$ and $Cl^-(H_2O) + CH_3Br$ reactions, potential energy surface scans [57] were performed at the MP2/[**c**/**d**] level of theory to obtain information on the reorganization of the solvent molecule as the reaction proceeds.

For the $Cl^- + CH_3Cl$ reaction in the gas phase, a potential energy scan was performed at the MP2/**c** level of theory with the Cl···C distance as an adjustable parameter and allowing full optimization of all other degrees of freedom. Solvent effects in the condensed phase were taken into account by using the isodensity polarized continuum (IPC) model [58] at the MP2/**c** level of theory on optimized structures from the above mentioned scan. The solvents used were heptane, benzene, chloroform, THF, acetone, methanol, acetonitrile, DMSO, and water. The solvent was specified in the computation by including the dielectric constant (ε). For the $Cl^- + CH_3I$ and

$I^- + CH_3Cl$ reactions in acetone, and for the $F^- + CH_3Cl$, $F^- + CH_3Br$, $F^- + CH_3I$, $Cl^- + CH_3Br$,

$Br^- + CH_3Br$, and $I^- + CH_3F$ reactions in water, the activation energies were determined at the MP2/**c** and MP2/[**c**/**d**] levels of theory using the IPC model.

4. Results and discussion

4.1. Structures

In Table 2 it can be seen that in general the MP2 optimized geometries for the three methyl halides and the five solvent molecules agree well with available experimental data [59]. The results from the HF geometries also show acceptable agreement. It should be noted that higher levels of theory would most probably give results that are in closer agreement with experimental data, but for the objectives of this study the results obtained are sufficiently accurate to provide good qualitative and quantitative insights. Upon chloride ion complex formation, some geometrical changes take place in the solvent molecules, but no dramatic or unexpected changes are observed. These results are summarized in Table 3. It is interesting to note that chloride ion interacts with only one hydrogen atom of NH_3, while it actually interacts with two hydrogen atoms of PH_3.

Many results on the geometries of the S_N2 ion–molecule complexes $X^-(CH_3Y)$ have previously been reported in the literature using a large variety of methods and basis sets [60–64]. The present results in Table 4 are almost identical to the results from the extensive studies of Glukhovtsev et al. [61,63].

Table 3
Computational MP2/**a** structural data for the chloride ion–solvent molecule complexes

Complex	Length (Å)/angle (°)	MP2
$Cl^-(H_2O)$	$Cl^-\cdots H$	2.191
	O–H	0.986/0.963
	H–O–H	101.5
$Cl^-(H_2S)$	$Cl^-\cdots H$	2.169
	S–H	1.368/1.330
	H–S–H	93.1
$Cl^-(NH_3)$	$Cl^-\cdots H$	2.246
	N–H	1.025/1.014
	H–N–H	105.2/106.1
$Cl^-(PH_3)$	$Cl^-\cdots H$	3.109/3.210
	P–H	1.398/1.418
	H–P–H	95.8
$Cl^-(SO_2)$	$Cl^-\cdots S$	2.667
	S–O	1.492
	O–S–O	115.2
$Br^-(H_2O)$	$Br^-\cdots H$	2.456
	O–H	0.989/0.971
	H–O–H	101.5

The solvated S_N2 complexes, $(S)X^-(CH_3Y)$ are far more interesting from a chemical point of view, and a large variation in structures can actually be observed. In Fig. 2 the MP2 structures of the $(S)Cl^-(CH_3Cl)$ complexes ($S = H_2O$, H_2S, NH_3, PH_3, SO_2) are shown. These reveal very different bonding characteristics particularly relative to the $Cl^-(S)$

Table 2
Computational HF/**a**, HF/[**c**/**d**], MP2/**a**, and MP2/[**c**/**d**] and experimental structural data for the solvent and methyl halide molecules studied

Molecule	Length (Å)/angle (°)	HF	MP2	Experiment[a]
CH_3Cl	C–H	1.078	1.085	1.11 ± 0.01
	C–Cl	1.786	1.778	1.784 ± 0.003
	H–C–H	110.6	110.0	110 ± 2
CH_3Br[b]	C–H	1.076	1.088	1.086
	C–Br	1.954	1.952	1.933
	H–C–H	111.1	110.9	111.2
CH_3I[b]	C–H	1.077	1.088	1.084
	C–I	2.148	2.146	2.132
	H–C–H	111.2	111.0	111.2
H_2O	O–H	0.943	0.963	0.958
	H–O–H	107.1	105.4	104.45
H_2S	S–H	1.327	1.331	1.3455
	H–S–H	94.4	92.9	93.3
NH_3	N–H	1.000	1.012	1.008 ± 0.004
	H–N–H	108.9	108.1	107.3 ± 0.2
PH_3	P–H	1.405	1.406	1.415 ± 0.003
	H–P–H	95.7	94.7	93.3 ± 0.2
SO_2	S–O	1.415	1.482	1.4321
	O–S–O	118.6	119.3	119.536

[a] From ref. [59].
[b] [**c**/**d**].

Table 4
Computational MP2/**a** and MP2/[**c**/**d**] structural data for the solvated and unsolvated S_N2 complexes

$X^-(CH_3Y)$	Length (Å)	MP2	$(S)X^-(CH_3Y)$	Length (Å)	MP2	$(S)X^-(CH_3Y)$	Length (Å)	MP2
Cl^- (CH_3Cl)	Cl···C	3.256	$(H_2O)Cl^-(CH_3Cl)$	Cl···C	3.269	$(H_2O)Cl^-$ (CH_3Br)	Cl···C	3.233
	C—Cl	1.808		C—Cl	1.804		C—Br	1.983
Cl^- (CH_3Br)	Cl···C	3.201		H···Cl	2.198		H···Cl	2.239
	C—Br	1.990	$(H_2S)Cl^-(CH_3Cl)$	Cl···C	3.265	$(H_2O)Br^-$ (CH_3Cl)	Br···C	3.455
Br^- (CH_3Cl)	Br···C	3.453		C—Cl	1.804		C—Cl	1.804
	C—Cl	1.808		H···Cl	2.195		H···Br	2.482
			$(NH_3)Cl^-(CH_3Cl)$	Cl···C	3.261			
				C—Cl	1.806			
				H···Cl	2.423			
			$(PH_3)Cl^-(CH_3Cl)$	Cl···C	3.261			
				C—Cl	1.806			
				H···Cl	2.502			
			$(SO_2)Cl^-(CH_3Cl)$	Cl···C	3.512			
				C—Cl	1.799			
				S···Cl	2.651			

complexes, but also relative to $Cl^-(CH_3Cl)$, especially in the case of $(SO_2)Cl^-(CH_3Cl)$. For S = H_2O, H_2S, NH_3, and PH_3 the $Cl^-(CH_3Cl)$ moiety does not change significantly relative to isolated $Cl^-(CH_3Cl)$. However, for $(SO_2)Cl^-(CH_3Cl)$ a large increase in the $Cl^-\cdots CH_3Cl$ distance takes place, from 3.256 to 3.512 Å. Other interesting features in this structure are the interaction of the two oxygen atoms of SO_2 with two hydrogen atoms of CH_3Cl (R(O···H) = 2.368 Å),

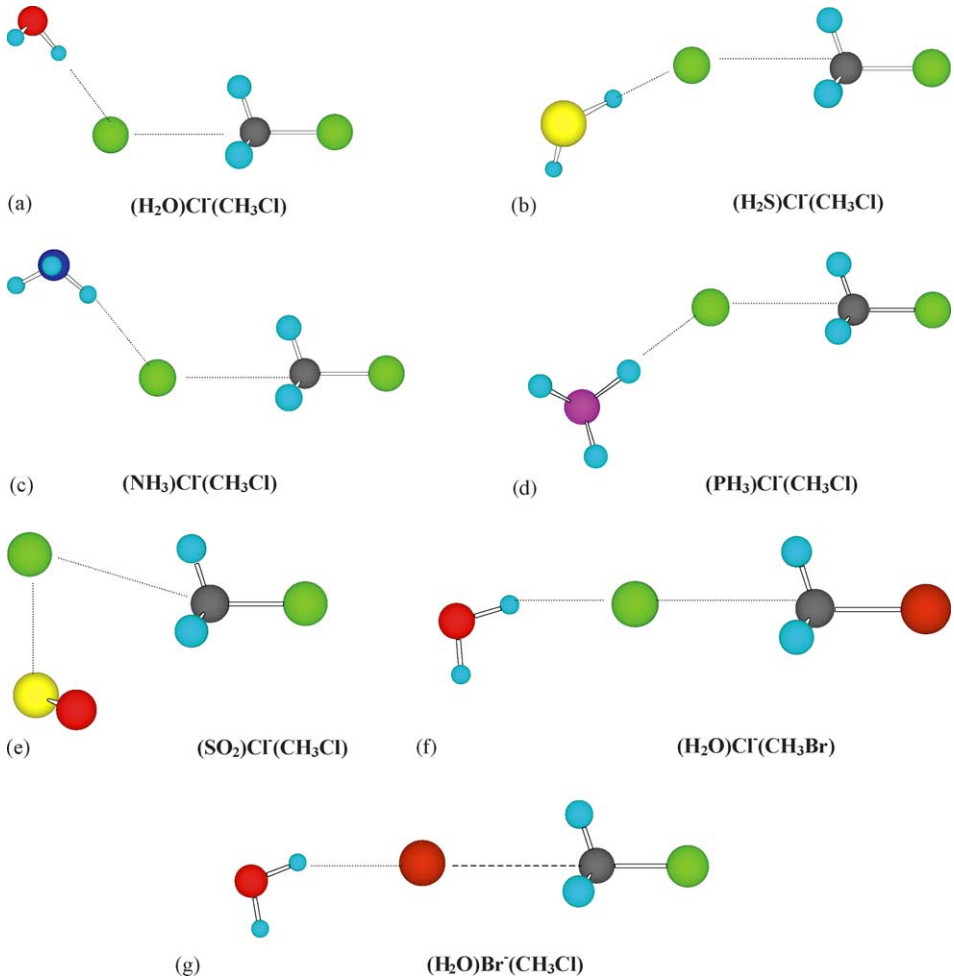

Fig. 2. Optimized MP2/**a** structure of (a) $(H_2O)Cl^-(CH_3Cl)$; (b) $(H_2SCl^-(CH_3Cl)$; (c) $(NH_3)Cl^-(CH_3Cl)$; (d) $(PH_3)Cl^-(CH_3Cl)$ and (e) $(SO_2)Cl^-(CH_3Cl)$. Optimized MP2/[**c**/**d**] structure of (f) $(H_2O)Cl^-(CH_3Br)$ and (g) $(H_2O)Br^-(CH_3Cl)$.

as well as the interaction of the chloride ion with the third hydrogen atom ($R(Cl^{-}\cdots H) = 3.046$ Å). H_2O and H_2S bind almost identically to $Cl^{-}(CH_3Cl)$, although the MP2 structures are quite different from the HF structures, with the latter being more symmetric. Except for $S = H_2O$, the other three hydrogen bonding solvents show an expected increase in the $Cl^{-}\cdots H$ distance. In contrast to $Cl^{-}(PH_3)$, in $(PH_3)Cl^{-}(CH_3Cl)$ the PH_3 molecule is bonded to chloride ion by only one hydrogen atom. Surprisingly, for the $(H_2O)Cl^{-}(CH_3Br)$ complex a more symmetric structure was obtained (Fig. 2(f)). However, it should be emphasized that the potential energy surface for the solvent molecule motion is fairly flat, and consequently the solvent molecule will be fairly mobile, giving rise to various shallow minima and considerable freedom of movement of the solvent molecule within the complex. Similarly to the chloride ion complex, the $(H_2O)Br^{-}(CH_3Cl)$ complex (Fig. 2(g)) has a symmetric structure with the $Cl^{-}(CH_3Br)$ and $Br^{-}(H_2O)$ moieties in this complex being almost identical to those in the isolated complexes.

For the transition states $[XCH_3Y]^{-\ddagger}$ similar comments can be made to those advanced for the analogous ion–molecule complexes. The structures of the solvated S_N2 transition states $[(S)ClCH_3Cl]^{-\ddagger}$ are shown in Fig. 3 and some of the key bond distances are summarized in Table 5. For $S = H_2O$ and H_2S relatively symmetric structures are obtained. In $[(H_2S)ClCH_3Cl]^{-\ddagger}$ the hydrogen atom not only interacts with the chloride on the left side, but also with that on the right side. However, it cannot be confidently concluded that for $S = H_2S$ transfer of the solvent molecule from the nucleophile to the leaving group would necessarily be more facile. This type of structure is not seen in these calculations for $S = H_2O$, however Morokuma [27] and Tucker and Truhlar [34] did find a bridge-like transition state for $S = H_2O$, in which the two hydrogen atoms are interacting with the two chlorides. Attempts to find similar structures failed at the MP2/**a** level of theory. The bonding of NH_3 and PH_3 is very different, with NH_3 bonding being more like that in the H_2O and H_2S transition states. As in the solvated S_N2 complex, PH_3 only binds via a single hydrogen atom in the solvated transition state. The binding of SO_2 in $[(SO_2)ClCH_3Cl]^{-\ddagger}$ is very different than that in $(SO_2)Cl^{-}(CH_3Cl)$. As expected, $R(S\cdots Cl)$ has increased, from 2.651 to 2.959 Å and only one oxygen atom interacts with one hydrogen atom at $R(O\cdots H) = 2.731$ Å. From all of these structures it seems that upon going from the solvated S_N2 complex to the transition state, for all solvents, a significant reorganization in the relative orientation of the solvent molecule takes place. Transition state structures $[(H_2O)_nClCH_3Cl]^{-\ddagger}$ with $n = 1$–3 have also been reported, and various isomers are possible [34,38]. It seems reasonable to assume that in the condensed phase extensive solvation of the transition state occurs, and that solvent reorganization is very complex. Nonetheless, information on the mono-solvated transition state may still provide some insight into the bulk behaviour, and even at this level reveals differences among solvents. For the water mono-solvated $[ClCH_3Br]^{-\ddagger}$ transition state, two isomers are possible, $[(H_2O)ClCH_3Br]^{-\ddagger}$and $[(H_2O)BrCH_3Cl]^{-\ddagger}$ (Fig. 3(f) and (g)). The halide bonded to the water molecule has a shorter distance to the carbon atom than that in $[ClCH_3Br]^{-\ddagger}$, while the other halide atom will be further away from the carbon atom. As expected, $R(H\cdots X)$ will be shorter for X = Cl than for Br, and this will have consequences for the solvation energy (see below). Finally, it should be noted that increasing the number of solvent molecules could provide additional insight in the cooperative binding of the solvent molecules in both the ion–molecule complexes and transition states.

4.2. Experimental thermochemistry

In Tables 6–9 the experimental PHPMS thermochemical data derived from this work on solvated S_N2 complexes together with that for other relevant species from the literature are shown. The corresponding van't Hoff plots for each of the clustering reactions studied are shown in Fig. 4. *Iso*-propyl chloride and bromide were chosen as the prototype

Table 5
Computational MP2/a and MP2/[c/d] structural data for the solvated and unsolvated S_N2 transition states

$[XCH_3Y]^{-}$	Length (Å)	MP2	$[(S)XCH_3Y]^{-}$	Length (Å)	MP2	$[(S)XCH_3Y]^{-}$	Length (Å)	MP2
$[ClCH_3Cl]^{-}$	Cl···C	2.310	$[(H_2O)ClCH_3Cl]^{-}$	Cl···C	2.265	$[(H_2O)ClCH_3Br]^{-}$	Cl···C	2.317
	C···Cl	2.311		C···Cl	2.348		Cl···Br	2.474
$[ClCH_3Br]^{-}$	Cl···C	2.371		H···Cl	2.294		H···Cl	2.308
	C···Br	2.430	$[(H_2S)ClCH_3Cl]^{-}$	Cl···C	2.277	$[(H_2O)BrCH_3Cl]^{-}$	Br···C	2.394
$[ClCH_2CNBr]^{-}$	Cl···C	2.365		C···Cl	2.333		Cl···Cl	2.398
	C···Br	2.440		H···Cl	2.443		H···Br	2.582
$[ClCH_3I]^{-}$	Cl···C	2.414	$[(NH_3)ClCH_3Cl]^{-}$	Cl···C	2.288	$[(H_2O)ClCH_2CNBr]^{-}$	Cl···C	2.317
	C···I	2.588		C···Cl	2.329		C···Br	2.476
				H···Cl	2.536		H···Cl	2.453
			$[(PH_3)ClCH_3Cl]^{-}$	Cl···C	2.288			
				C···Cl	2.332			
				H···Cl	2.650			
			$[(SO_2)ClCH_3Cl]^{-}$	Cl···C	2.232			
				C···Cl	2.387			
				S···Cl	2.959			

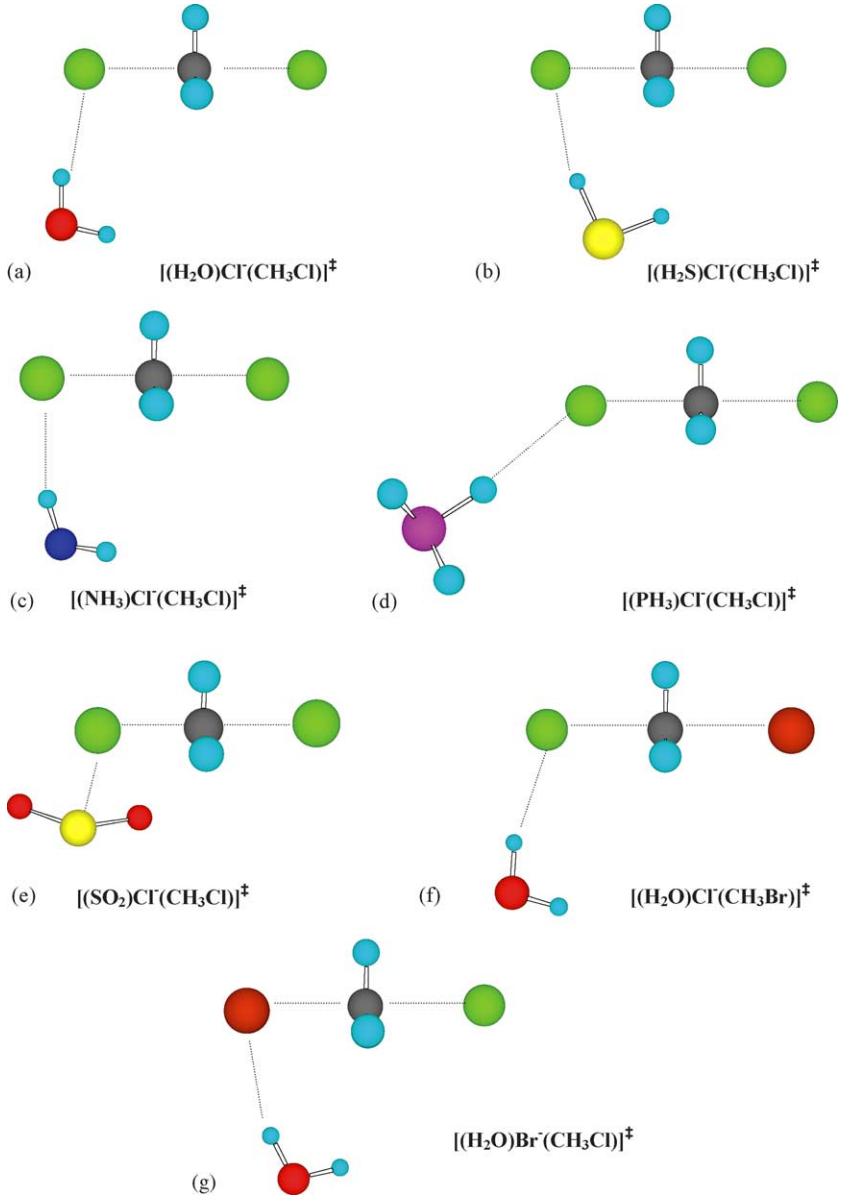

Fig. 3. Optimized MP2/**a** structure of (a) $[(H_2O)ClCH_3Cl]^{-‡}$; (b) $[(H_2S)ClCH_3Cl]^{-‡}$; (c) $[(NH_3)ClCH_3Cl]^{-‡}$; (d) $[(PH_3)ClCH_3Cl]^{-‡}$ and (e) $[(SO_2)ClCH_3Cl]^{-‡}$. Optimized MP2/[**c**/**d**] structure of (f) $[(H_2O)ClCH_3Br]^{-‡}$ and (g) $[(H_2O)BrCH_3Cl]^{-‡}$.

Table 6
Experimental PHPMS thermochemistry for the $X^- + S \rightleftharpoons X^-(S)$ (X = Cl, Br; S = CH_3OH, CH_3CN, $(CH_3)_2CO$, CH_3CF_2H) and $X^- + RY \rightleftharpoons X^-(RY)$ (X, Y = Cl, Br; R = $(CH_3)_2CH$) clustering equilibria

System#	Clustering equilibrium	ΔH° (kcal mol^{-1})	ΔS° (cal mol^{-1} K^{-1})	Reference
	$Cl^- + (CH_3)_2CHCl \rightleftharpoons Cl^-((CH_3)_2CHCl)$	−14.7	−23.3	[65]
	$Cl^- + (CH_3)_2CHBr \rightleftharpoons Cl^-((CH_3)_2CHBr)$	−15.2	−24.0	[65]
	$Cl^- + CH_3OH \rightleftharpoons Cl^-(CH_3OH)$	−17.5	−24.0	[71]
	$Cl^- + CH_3CN \rightleftharpoons Cl^-(CH_3CN)$	−15.8	−18.7	[65]
1	$Cl^- + (CH_3)_2CO \rightleftharpoons Cl^-((CH_3)_2CO)$	−14.1	−20.2	This work
2	$Cl^- + CH_3CF_2H \rightleftharpoons Cl^-(CH_3CF_2H)$	−12.8	−18.4	This work
	$Br^- + (CH_3)_2CHCl \rightleftharpoons Br^-((CH_3)_2CHCl)$	−12.4	−20.6	[65]
	$Br^- + CH_3OH \rightleftharpoons Br^-(CH_3OH)$	−14.5	−21.9	[73]
	$Br^- + CH_3CN \rightleftharpoons Br^-(CH_3CN)$	−14.3	−18.7	[65]
3	$Br^- + (CH_3)_2CO \rightleftharpoons Br^-((CH_3)_2CO)$	−11.2	−15.9	This work
4	$Br^- + CH_3CF_2H \rightleftharpoons Br^-(CH_3CF_2H)$	−10.6	−15.7	This work

Estimated relative errors: ΔH° ±0.2 kcal mol^{-1}; ΔS° ± 1.0 cal mol^{-1} K^{-1}. Estimated absolute errors: ΔH° ± 0.4 kcal mol^{-1}; ΔS° ± 2.0 cal mol^{-1} K^{-1}.

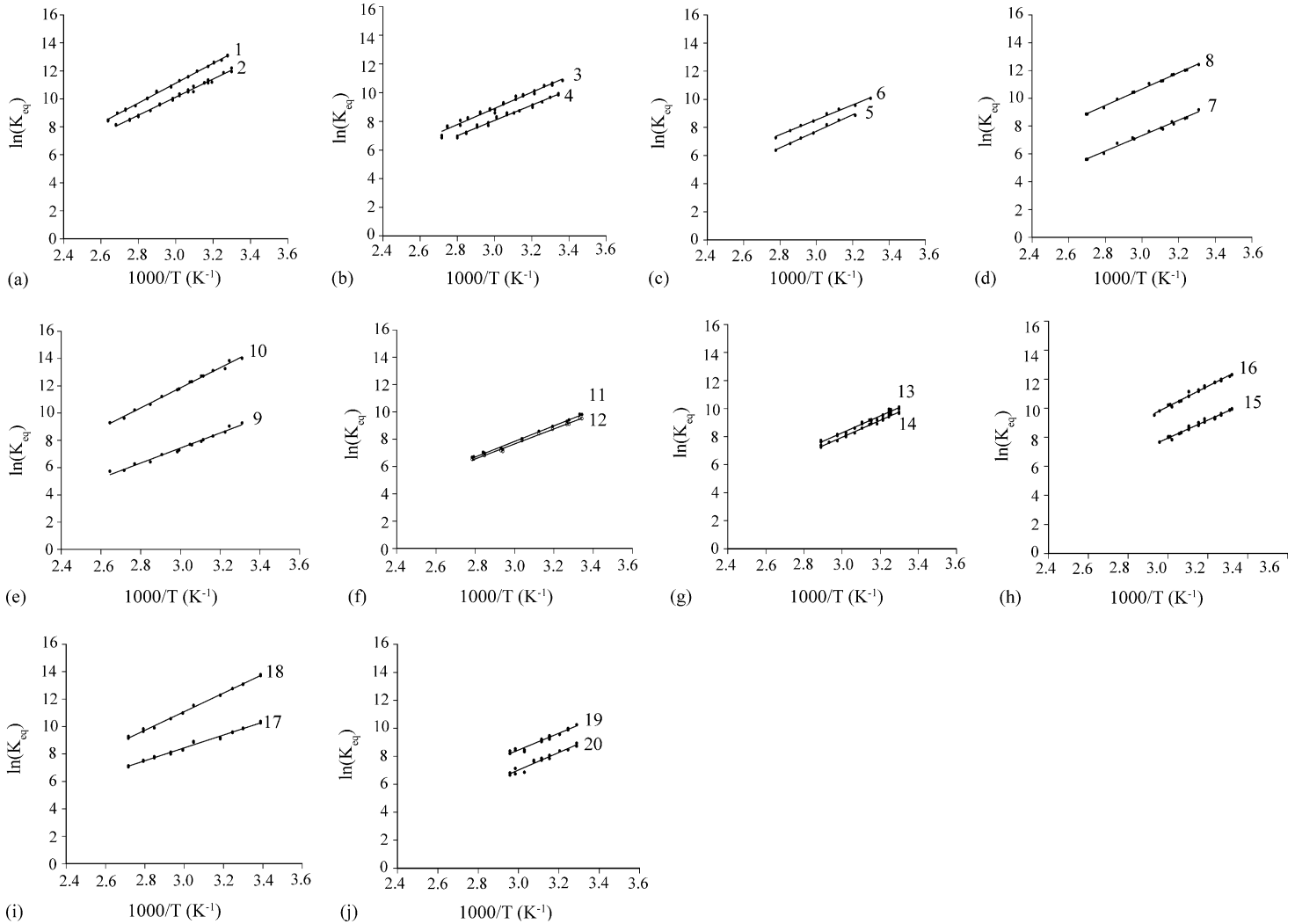

Fig. 4. van't Hoff plots for (a) the $Cl^- + S \rightleftharpoons Cl^-(S)$ ($S = (CH_3)_2CO$, CH_3CF_2H) clustering equilibria; (b) the $Br^- + S \rightleftharpoons Br^-(S)$ ($S = (CH_3)_2CO$, CH_3CF_2H) clustering equilibria; (c) the $Cl^-(S) + RCl \rightleftharpoons (S)Cl^-(RCl)$ and $Cl^-(RCl) + S \rightleftharpoons (S)Cl^-(RCl)$ ($S = CH_3OH$; $R = (CH_3)_2CH$) clustering equilibria; (d) the $Cl^-(S) + RCl \rightleftharpoons (S)Cl^-(RCl)$ and $Cl^-(RCl) + S \rightleftharpoons (S)Cl^-(RCl)$ ($S = CH_3CN$; $R = (CH_3)_2CH$) clustering equilibria; (e) the $Cl^-(S) + RCl \rightleftharpoons (S)Cl^-(RCl)$ and $Cl^-(RCl) + S \rightleftharpoons (S)Cl^-(RCl)$ ($S = (CH_3)_2CO$; $R = (CH_3)_2CH$) clustering equilibria; (g) the $Cl^-(S) + RCl \rightleftharpoons (S)Cl^-(RCl)$ and $Cl^-(RCl) + S \rightleftharpoons (S)Cl^-(RCl)$ ($S = CH_3CF_2H$; $R = (CH_3)_2CH$) clustering equilibria; (h) the $Cl^-(S) + RBr \rightleftharpoons (S)Cl^-(RBr)$ and $Cl^-(RBr) + S \rightleftharpoons (S)Cl^-(RBr)$ ($S = CH_3OH$; $R = (CH_3)_2CH$) clustering equilibria; (i) the $Cl^-(S) + RBr \rightleftharpoons (S)Cl^-(RBr)$ and $Cl^-(RBr) + S \rightleftharpoons (S)Cl^-(RBr)$ ($S = CH_3CN$; $R = (CH_3)_2CH$) clustering equilibria; (j) the $Cl^-(S) + RBr \rightleftharpoons (S)Cl^-(RBr)$ and $Cl^-(RBr) + S \rightleftharpoons (S)Cl^-(RBr)$ ($S = (CH_3)_2CO$; $R = (CH_3)_2CH$) clustering equilibria; (k) the $Cl^-(S) + RBr \rightleftharpoons (S)Cl^-(RBr)$ and $Cl^-(RBr) + S \rightleftharpoons (S)Cl^-(RBr)$ ($S = CH_3CF_2H$; $R = (CH_3)_2CH$) clustering equilibria.

Table 7
Experimental PHPMS thermochemistry for the $Cl^-(S) + RCl \rightleftharpoons (S)Cl^-(RCl)$ and $Cl^-(RCl) + S \rightleftharpoons (S)Cl^-(RCl)$ (S = CH_3OH, CH_3CN, $(CH_3)_2CO$, CH_3CF_2H; R = $(CH_3)_2CH$) clustering equilibria

System#	Clustering equilibrium	ΔH° (kcal mol^{-1})	ΔS° (cal mol^{-1} K^{-1})
5	$Cl^-(CH_3OH) + (CH_3)_2CHCl \rightleftharpoons (CH_3OH)Cl^-((CH_3)_2CHCl)$	−11.0	−18.1
6	$Cl^-((CH_3)_2CHCl) + CH_3OH \rightleftharpoons (CH_3OH)Cl^-((CH_3)_2CHCl)$	−14.6	−20.3
7	$Cl^-(CH_3CN) + (CH_3)_2CHCl \rightleftharpoons (CH_3CN)Cl^-((CH_3)_2CHCl)$	−11.0	−18.5
8	$Cl^-((CH_3)_2CHCl) + CH_3CN \rightleftharpoons (CH_3CN)Cl^-((CH_3)_2CHCl)$	−11.7	−13.8
9	$Cl^-((CH_3)_2CO) + (CH_3)_2CHCl \rightleftharpoons ((CH_3)_2CO)Cl^-((CH_3)_2CHCl)$	−11.7	−19.7
10	$Cl^-((CH_3)_2CHCl) + (CH_3)_2CO \rightleftharpoons ((CH_3)_2CO)Cl^-((CH_3)_2CHCl)$	−10.5	−14.4
11	$Cl^-(CH_3CF_2H) + (CH_3)_2CHCl \rightleftharpoons (CH_3CF_2H)Cl^-((CH_3)_2CHCl)$	−11.3	−18.4
12	$Cl^-((CH_3)_2CHCl) + CH_3CF_2H \rightleftharpoons (CH_3CF_2H)Cl^-((CH_3)_2CHCl)$	−10.9	−17.5

Estimated relative errors: $\Delta H^\circ \pm 0.2$ kcal mol^{-1}, $\Delta S^\circ \pm 1.0$ cal mol^{-1} K^{-1}. Estimated absolute errors $\Delta H^\circ \pm 0.4$ kcal mol^{-1}; $\Delta S^\circ \pm 2.0$ cal mol^{-1} K^{-1}.

Table 8
Experimental PHPMS thermochemistry for the $Cl^-(S) + RBr \rightleftharpoons (S)Cl^-(RBr)$ and $Cl^-(RBr) + S \rightleftharpoons (S)Cl^-(RBr)$ (S = CH_3OH, CH_3CN, $(CH_3)_2CO$, CH_3CF_2H; R = $(CH_3)_2CH$) clustering equilibria

System#	Clustering equilibrium	ΔH° (kcal mol^{-1})	ΔS° (cal mol^{-1} K^{-1})
13	$Cl^-(CH_3OH) + (CH_3)_2CHBr \rightleftharpoons (CH_3OH)Cl^-((CH_3)_2CHBr)$	−11.8	−21.0
14	$Cl^-((CH_3)_2CHBr) + CH_3OH \rightleftharpoons (CH_3OH)Cl^-((CH_3)_2CHBr)$	−14.8	−22.9
15	$Cl^-(CH_3CN) + (CH_3)_2CHBr \rightleftharpoons (CH_3CN)Cl^-((CH_3)_2CHBr)$	−12.3	−21.1
16	$Cl^-((CH_3)_2CHBr) + CH_3CN \rightleftharpoons (CH_3CN)Cl^-((CH_3)_2CHBr)$	−13.9	−21.5
17	$Cl^-((CH_3)_2CO) + (CH_3)_2CHBr \rightleftharpoons ((CH_3)_2CO)Cl^-((CH_3)_2CHBr)$	−11.9	−19.4
18	$Cl^-((CH_3)_2CHBr) + (CH_3)_2CO \rightleftharpoons ((CH_3)_2CO)Cl^-((CH_3)_2CHBr)$	−11.9	−20.0
19	$Cl^-(CH_3CF_2H) + (CH_3)_2CHBr \rightleftharpoons (CH_3CF_2H)Cl^-((CH_3)_2CHBr)$	−11.9	−18.8
20	$Cl^-((CH_3)_2CHBr) + CH_3CF_2H \rightleftharpoons (CH_3CF_2H)Cl^-((CH_3)_2CHBr)$	−12.4	−23.4

Estimated relative errors: $\Delta H^\circ \pm 0.2$ kcal mol^{-1}; $\Delta S^\circ \pm 1.0$ cal mol^{-1} K^{-1}. Estimated absolute errors: $\Delta H^\circ \pm 0.4$ kcal mol^{-1}; $\Delta S^\circ \pm 2.0$ cal mol^{-1} K^{-1}.

alkyl halides for this study in order that the binding energetics of the three component complexes would be sufficient to permit equilibrium measurements to be made over an adequate temperature range. In addition, in order that the S_N2 displacement reaction of the unsolvated species be sufficiently slow that no complications due to its occurrence interfere with the clustering measurements, *iso*-propyl bromide was taken as the only viable choice for the non-identity reaction. This is a consequence of the fact that the barrier to this reaction lies above the energy of reactants whereas for both methyl and ethyl bromides the barrier lies below the energy of reactants. For solvents, methanol was chosen as a prototypical protic species, acetonitrile and acetone were chosen as typical dipolar aprotic solvents and CH_3CF_2H was chosen as an, albeit poor, model of a hydrocarbon solvent.

In previous work from this laboratory Li et al. [65] determined the well-depths and transition state energies for several S_N2 reactions using similar PHPMS experiments and some of these data relevant to the present study are also summarized in Table 6. As noted above, there are two different reactions that can take place leading to the solvated S_N2 complex $(S)X^-(RY)$, Eqs. (3) and (4). A thermochemical cycle for the formation of the $(S)X^-(RY)$ complex from separated reactants, X^-, RY, and S, which relates the thermochemical values for the two different routes to the solvated complexes

Table 9
Experimental PHPMS thermochemistry for the $Br^-(S) + RCl \rightleftharpoons (S)Br^-(RCl)$ and $Br^-(RCl) + S \rightleftharpoons (S)Br^-(RCl)$ (S = CH_3OH, CH_3CN, $(CH_3)_2CO$, CH_3CF_2H; R = $(CH_3)_2CH$) clustering equilibria

Clustering equilibrium	ΔG°_{300} (kcal mol^{-1})	ΔH° (kcal mol^{-1})	ΔS° (cal mol^{-1} K^{-1})
$Br^-(CH_3OH) + (CH_3)_2CHCl \rightleftharpoons (CH_3OH)Br^-((CH_3)_2CHCl)$	−4.9	−10.6	−18.0
$Br^-((CH_3)_2CHCl) + CH_3OH \rightleftharpoons (CH_3OH)Br^-((CH_3)_2CHCl)$	−7.0	−12.4	−18.0
$Br^-(CH_3CN) + (CH_3)_2CHCl \rightleftharpoons (CH_3CN)Br^-((CH_3)_2CHCl)$	−4.5	−9.9	−18.0
$Br^-((CH_3)_2CHCl) + CH_3CN \rightleftharpoons (CH_3CN)Br^-((CH_3)_2CHCl)$	−6.4	−12.0	−18.0
$Br^-((CH_3)_2CO) + (CH_3)_2CHCl \rightleftharpoons ((CH_3)_2CO)Br^-((CH_3)_2CHCl)$	−5.0	−10.4	−18.0
$Br^-((CH_3)_2CHCl) + (CH_3)_2CO \rightleftharpoons ((CH_3)_2CO)Br^-((CH_3)_2CHCl)$	−5.3	−10.7	−18.0
$Br^-(CH_3CF_2H) + (CH_3)_2CHCl \rightleftharpoons (CH_3CF_2H)Br^-((CH_3)_2CHCl)$	−5.0	−10.4	−18.0
$Br^-((CH_3)_2CHCl) + CH_3CF_2H \rightleftharpoons (CH_3CF_2H)Br^-((CH_3)_2CHCl)$	−4.8	−10.2	−18.0

Estimated relative errors: $\Delta G^\circ_{300} \pm 0.2$ kcal mol^{-1}; $\Delta H^\circ \pm 0.5$ kcal mol^{-1}; $\Delta S^\circ \pm 1.0$ cal mol^{-1} K^{-1}. Estimated absolute errors: $\Delta G^\circ_{300} \pm 0.4$ kcal mol^{-1}; $\Delta H^\circ \pm 1.0$ kcal mol^{-1}; $\Delta S^\circ \pm 2.0$ cal mol^{-1} K^{-1}.

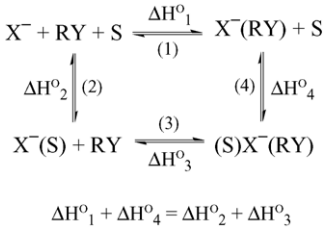

Fig. 5. Thermochemical cycle for the formation of solvated S_N2 complexes.

is shown in Fig. 5. Using the data in Tables 6–9 the energetics for the formation of the solvated S_N2 complexes can be calculated by the two different routes. For the Cl^-/CH_3OH, CH_3CN and $(CH_3)_2CO/(CH_3)_2CHCl$ systems the agreement following these two pathways is generally very good and the conclusion can be drawn that the structures of the solvated S_N2 complexes formed are independent of the path followed. However, the same cannot be said for the $Cl^-/CH_3CF_2H/(CH_3)_2CHCl$, $Cl^-/CH_3CF_2H/(CH_3)_2CHBr$ and $Br^-/(CH_3)_2CO$, $CH_3CF_2H/(CH_3)_2CHBr$ systems. These cases represent situations where the alkyl halide binds the relevant halide ion more strongly than the solvent molecule. It might then be anticipated that the addition of the solvated halide ion to the alkyl halide is accompanied effectively by a halide ion transfer to the alkyl halide and subsequent solvation of that complex. The fact that the two routes through the thermochemical cycle do not give the same energetic changes would suggest that possibly the situation is not this simple. A comparison of the data in Tables 8 and 9 reveals that the enthalpy changes for complexation for the four special cases above are less favourable than expected, which leads to the possibility that this halide ion transfer is not occurring and that more than one possible structure of the solvated complex might be formed. It is known that proton transfer involving carbon acids frequently involves substantial barriers and thus a complex of halide ion, alkyl halide and solvent which exists in a double well with a substantial barrier between the minima is not unreasonable. Unfortunately the substantial computer resources necessary to test this hypothesis via ab initio calculations were not available to us. It is quite noteworthy however that the trends in energetics with changing solvent for analogous reactions reveals no strong differences among the four prototypical solvents investigated.

Table 11
Computational MP2//MP2 ΔH^{circ}_{298} values for the $X^-(S) + CH_3Y \rightleftharpoons (S)X^-(CH_3Y)$ and $X^-(CH_3Y) + S \rightleftharpoons (S)X^-(CH_3Y)$ (X = Cl, Br; Y = Cl, Br, I; S = H_2O, H_2S, NH_3, PH_3, SO_2, CH_3OCH_3) clustering equilibria

Clustering equilibrium	ΔH°_{298}, MP2//MP2 (kcal mol^{-1})
$Cl^-(H_2O) + CH_3Cl \rightleftharpoons (H_2O)Cl^-(CH_3Cl)$	−8.5
$Cl^-(CH_3Cl) + H_2O \rightleftharpoons (H_2O)Cl^-(CH_3Cl)$	−12.6
$Cl^-(H_2S) + CH_3Cl \rightleftharpoons (H_2S)Cl^-(CH_3Cl)$	−8.3
$Cl^-(CH_3Cl) + H_2S \rightleftharpoons (H_2S)Cl^-(CH_3Cl)$	−10.7
$Cl^-(NH_3) + CH_3Cl \rightleftharpoons (NH_3)Cl^-(CH_3Cl)$	−8.9
$Cl^-(CH_3Cl) + NH_3 \rightleftharpoons (NH_3)Cl^-(CH_3Cl)$	−6.6
$Cl^-(PH_3) + CH_3Cl \rightleftharpoons (PH_3)Cl^-(CH_3Cl)$	−9.6
$Cl^-(CH_3Cl) + PH_3 \rightleftharpoons (PH_3)Cl^-(CH_3Cl)$	−4.5
$Cl^-(SO_2) + CH_3Cl \rightleftharpoons (SO_2)Cl^-(CH_3Cl)$	−9.1
$Cl^-(CH_3Cl) + SO_2 \rightleftharpoons (SO_2)Cl^-(CH_3Cl)$	−20.0
$Cl^-(H_2O) + CH_3Br \rightleftharpoons (H_2O)Cl^-(CH_3Br)$	−8.3
$Cl^-(CH_3Br) + H_2O \rightleftharpoons (H_2O)Cl^-(CH_3Br)$	−12.4
$Cl^-(CH_3OCH_3) + CH_3I \rightleftharpoons (CH_3OCH_3)Cl^-(CH_3I)$	−9.8
$Cl^-(CH_3I) + CH_3OCH_3 \rightleftharpoons (CH_3OCH_3)Cl^-(CH_3I)$	−7.1
$Br^-(H_2O) + CH_3Cl \rightleftharpoons (H_2O)Br^-(CH_3Cl)$	−8.4
$Br^-(CH_3Cl) + H_2O \rightleftharpoons (H_2O)Br^-(CH_3Cl)$	−10.9

4.3. Computational thermochemistry

In Table 10, the computational thermochemistry for a large variety of halide ion–solvent molecule and S_N2 substrate clustering equilibria, together with available experimental data [65,66] are shown. In general, the agreement between ΔH°_{298} values from the MP2/**b**//MP2/**a** and G2(MP2)

Table 10
Computational and experimental literature thermochemical data for the $X^- + S \rightleftharpoons X^-(S)$ and $X^- + CH_3Y \rightleftharpoons X^-(CH_3Y)$ (X = Cl, Br; Y = Cl, Br, I; S = H_2O, H_2S, NH_3, PH_3, SO_2, CH_3OCH_3) clustering equilibria

Clustering equilibrium	ΔH°_{298} (kcal mol^{-1})		ΔH° (kcal mol^{-1})	ΔS°_{298} (cal mol^{-1} K^{-1})	ΔS° (cal mol^{-1} K^{-1})[a]
	MP2//MP2	G2(MP2)	PHPMS	HF	PHPMS
$Cl^- + H_2O \rightleftharpoons Cl^-(H_2O)$	−14.5	−14.2	−14.7[b]	−17.5	−19.7[b]
$Cl^- + H_2S \rightleftharpoons Cl^-(H_2S)$	−12.8	−12.5		−17.5	
$Cl^- + NH_3 \rightleftharpoons Cl^-(NH_3)$	−8.1	−8.0	−8.2[c]	−14.9	−15.4[c]
$Cl^- + PH_3 \rightleftharpoons Cl^-(PH_3)$	−5.3	−6.0		−14.0	
$Cl^- + SO_2 \rightleftharpoons Cl^-(SO_2)$	−21.3	−21.8	−22.2[c]	−21.4	−21.6[c]
$Cl^- + CH_3OCH_3 \rightleftharpoons Cl^-(CH_3OCH_3)$	−7.6		−7.5[d]	−19.0[a]	−15.3[d]
$Cl^- + CH_3Cl \rightleftharpoons Cl^-(CH_3Cl)$	−10.4	−10.7	−10.4[e]	−14.6	−15.3[e]
$Cl^- + CH_3Br \rightleftharpoons Cl^-(CH_3Br)$	−10.4		−12.5[e]	−14.9	
$Cl^- + CH_3I \rightleftharpoons Cl^-(CH_3I)$	−7.6		−9.8[f]	−14.9[a]	
$Br^- + H_2O \rightleftharpoons Br^-(H_2O)$	−13.2		−11.7[b]	−16.4	−14.7[b]
$Br^- + CH_3Cl \rightleftharpoons Br^-(CH_3Cl)$	−10.7		−10.9[e]	−13.6	−20.3[e]

[a]MP2/**a**, [b]From ref. [72], [c]From ref. [73], [d]From ref. [74], [e]From ref. [65], [f]From refs. [75,76].

computations and ΔH° values from PHPMS experiments are good to excellent. This gives some confidence that the results from the MP2/**b**//MP2/**a** for the solvated S_N2 systems should also give reliable results and trends. Entropy data are calculated using the standard statistical thermodynamic formulations for a rigid rotor, harmonic oscillator species. For the ΔS°_{298} values from HF/**a** computations and ΔS° values from PHPMS experiments the agreement is very much system dependent. Systems containing bromine and iodine atoms gave varying results. In general however, for most systems studied, the agreement with other available computational data was good. For some of the more weakly bound systems the calculated ΔS°_{298} values show substantial inconsistencies with the experimental PHPMS data. This is particularly true for the larger, more complex substrates. This is more than likely the result of the failure of the calculations to accurately reproduce low frequency intermolecular vibrational modes as well as the fact that treatment of these modes by the standard procedures does not take account of their anharmonic character. Additionally, particularly for more complex systems, the possibility of the presence of more than one conformational form could also contribute to any differences.

In Table 11 the ΔH°_{298} values for the formation of solvated S_N2 complexes from the MP2/**b**//MP2/**a** computations are shown. For the reasons noted above ΔS°_{298} values are not reported as they are expected to be significantly in error. Since only one structure of the solvated S_N2 complex has been investigated, these values all satisfy the thermochemical cycle in Fig. 5. As noted above, some structural changes can take place in the X^-(RY) complexes after addition of a solvent molecule, and this may give rise to unexpected ΔH° and ΔS° values.

Tucker and Truhlar [34] found a ΔH°_{298} value of -10.1 kcal mol^{-1}, at the MP2/6-31G(d,p) level of theory, for Eq. (27a) while for Eq. (27b) a ΔH°_{298} value of -9.3 kcal mol^{-1} was obtained.

$$Cl^-(H_2O) + CH_3Cl \rightleftharpoons (H_2O)Cl^-(CH_3Cl) \quad (27a)$$

$$Cl^-(H_2O)_2 + CH_3Cl \rightleftharpoons (H_2O)_2Cl^-(CH_3Cl) \quad (27b)$$

No other computations with other solvents than water are available for the X^-(S) + RY reactions.

In Table 12 the results of the $\Delta H^\ddagger_{298}$ values to go from the reactants to the transition states for selected unsolvated and solvated S_N2 reactions (Eqs. (28) and (29)) are given.

$$X^- + CH_3Y \rightleftharpoons [XCH_3Y]^{-\ddagger} \quad (28)$$

$$X^-(S) + CH_3Y \rightarrow [(S)XCH_3Y]^{-\ddagger} \quad (29)$$

The present values for Eq. (28) give reasonable to good agreement with available experimental and computational data. It can be seen that the $\Delta H^\ddagger_{298}$ values for S = H_2O and H_2S are nearly identical, while the same is true for S = NH_3 and PH_3. Tucker and Truhlar [34] found a $\Delta H^\ddagger_{298}$ value of +5.4 kcal mol^{-1} for Eq. (30) at the MP2/6-31G(d,p) level of theory, while for Eq. (31) a value of +10.7 kcal mol^{-1} was obtained.

$$Cl^-(H_2O) + CH_3Cl \rightarrow [(H_2O)ClCH_3Cl]^{-\ddagger} \quad (30)$$

$$Cl^-(H_2O)_2 + CH_3Cl \rightarrow [(H_2O)_2ClCH_3Cl]^{-\ddagger} \quad (31)$$

Introducing more solvent molecules will give rise to more solvated transition states as shown by Morokuma [27]. For instance, for Eq. (31), $[(H_2O)ClCH_3Cl(H_2O)]^{-\ddagger}$ would also

Table 12
Computational MP2//MP2 $\Delta H^\ddagger_{298}$ and experimental $\Delta H^\ddagger$ values for the X^- + Y = Cl, Br, I; Z = H, CN, S = H_2O, H_2S, NH_3, PH_3, SO_2) reactions

Reaction	ΔH°_{298}, MP2//MP2 (kcal mol^{-1})	$\Delta H^\#$, experiment (kcal mol^{-1})
$Cl^- + CH_3Cl \rightarrow [ClCH_3Cl]^-$	+4.5	+1.0 ± 1.0[a], +3.1[b], +2.5[c], 2.9 ± 1.0[d]
$Cl^- + CH_3Br \rightarrow [ClCH_3Br]^-$	+2.9	−1.8[e], −1.8[f],−1.7[d], −1.5[g], −1.1[c], −4.7[h]
$Cl^- + CH_3I \rightarrow [ClCH_3I]^-$	−0.1	−4.6 ± 0.5[d], −2.7[i]
$Cl^- + CH_2CNBr \rightarrow [ClCH_2CNBr]^-$	−5.6	−6.1[c]
$Br^- + CH_3Cl \rightarrow [ClCH_3Br]^-$	+3.1	+5.7[f]
$Br^- + CH_2CNCl \rightarrow [ClCH_2CNBr]^-$	−6.5	
$Cl^-(H_2O) + CH_3Cl \rightarrow H_2O)ClCH_3Cl]^-$	+9.0	
$Cl^-(H_2S) + CH_3Cl \rightarrow H_2S)ClCH_3Cl]^-$	+9.3	
$Cl^-(NH_3) + CH_3Cl \rightarrow [(NH_3)ClCH_3Cl]^-$	+7.2	
$Cl^-(PH_3) + CH_3Cl \rightarrow [(PH_3)ClCH_3Cl]^-$	+7.3	
$Cl^-(SO_2) + CH_3Cl \rightarrow [(SO_2)ClCH_3Cl]^-$	+15.5	
$Cl^-(H_2O) + CH_3Br \rightarrow [(H_2O)ClCH_3Br]^-$	+7.0	
$Cl^-(H_2O) + CH_2CNBr \rightarrow [(H_2O)ClCH_2CNBr]^-$	−1.3	
$Br^-(H_2O) + CH_3Cl \rightarrow [ClCH_3Br(H_2O)]^-$	+6.1	

[a] From ref. [77].
[b] From ref. [78].
[c] From ref. [79].
[d] From ref. [80].
[e] From ref. [81].
[f] From ref. [65].
[g] From ref. [82].
[h] From ref. [25].
[i] From ref. [83].

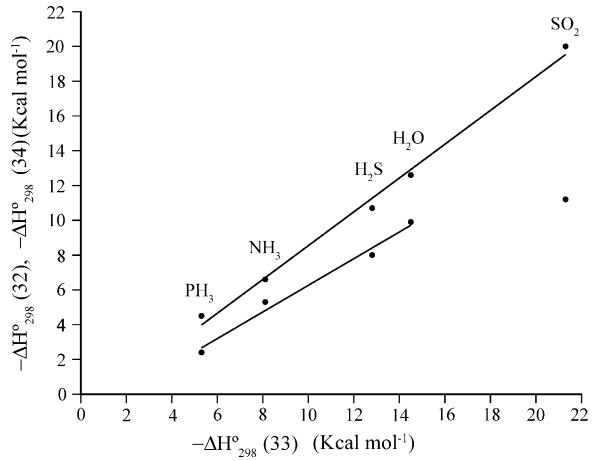

Fig. 6. Plot of $-\Delta H^{\circ}_{298}$ for the formation of $Cl^-(S)$ vs. $-\Delta H^{\circ}_{298}$ for the formation of $(S)Cl^-(CH_3Cl)$ and $[(S)ClCH_3Cl]^-$ (S = H_2O, H_2S, NH_3, PH_3, SO_2).

be a valid alternative. A different picture emerges if ΔH°_{298} for Eq. (32) is taken instead of $\Delta H^{\ddagger}_{298}$ for Eq. (29).

$$[ClCH_3Cl]^{-\ddagger} + S \rightleftharpoons [(S)ClCH_3Cl]^{-\ddagger} \quad (32)$$

For S = H_2O, H_2S, NH_3, PH_3, and SO_2 ΔH°_{298} values of −9.9, −8.0, −5.3, −2.4, and −11.2 kcal mol^{-1}, respectively, can be found. A plot the $-\Delta H^{\circ}_{298}$ values for Eq. (33) versus the $-\Delta H^{\circ}_{298}$ values for Eqs. (32) and (34), is shown in Fig. 6.

$$Cl^- + S \rightleftharpoons Cl^-(S) \quad (33)$$

$$Cl^-(CH_3Cl) + S \rightleftharpoons (S)Cl^-(CH_3Cl) \quad (34)$$

Interestingly, both plots show a linear correlation, except for the transition state solvation by SO_2. From these plots it can be seen that the solvation of the transition states is less exothermic than the solvation of the S_N2 ion–molecule complexes, which is in turn less exothermic than the solvation of the bare halide ion.

In Fig. 7 all data for Eqs. (17)–(19) from Tables 10–12 are shown together as schematic potential energy profiles. With the exception of PH_3 the transition states $[(S)ClCH_3Cl]^{-\ddagger}$ can all be seen to be lower in ΔH°_{298} value than the separated individual reactants, $Cl^- + CH_3Cl + S$. This means that it could be possible to kinetically excite $^{35}Cl^-(S)$, for instance, and to monitor formation of $^{37}Cl^-$ and/or $^{37}Cl^-(S)$ from these energetic collisions with CH_3Cl (Eq. (35a) and (35b)).

$$^{35}Cl^-(S) + CH_3{}^{37}Cl \rightarrow {}^{37}Cl^- + CH_3{}^{35}Cl + S \quad (35a)$$

$$^{35}Cl^-(S) + CH_3{}^{37}Cl \rightarrow {}^{37}Cl^-(S) + CH_3{}^{35}Cl \quad (35b)$$

Unfortunately, at lower centre-of-mass kinetic energies for $^{35}Cl^-(S)$, simple collision induced dissociation (reaction (36)) or chloride ion transfer to CH_3Cl (reaction (37)) may also occur.

$$^{35}Cl^-(S) + CH_3Cl \rightarrow {}^{35}Cl^- + S + CH_3Cl \quad (36)$$

$$^{35}Cl^-(S) + CH_3Cl \rightarrow {}^{35}Cl^-(CH_3Cl) + S \quad (37)$$

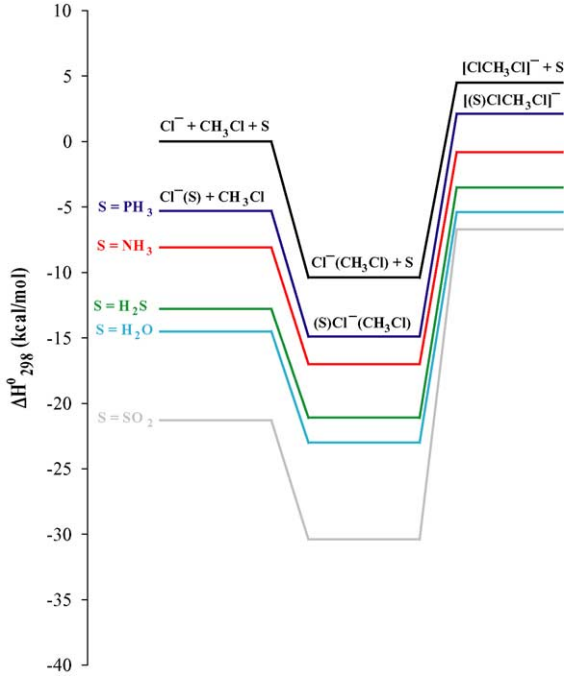

Fig. 7. Schematic MP2/**b**//MP2/**a** potential energy profiles for the $Cl^- + CH_3Cl$ and $Cl^-(S) + CH_3Cl$ reactions (S = H_2O, H_2S, NH_3, PH_3, SO_2).

For the water mono-solvated transition state of $[ClCH_3Br]^-$, two isomers are possible, $[(H_2O)ClCH_3Br]^-$ and $[(H_2O)BrCH_3Cl]^-$. At the MP2/[**b**/**e**]//MP2/[**c**/**d**] level of theory, including zero-point energies and thermal corrections at the MP2/[**c**/**d**] level of theory, the first of these is only 0.4 kcal mol^{-1} more favorable than the second. Still, the barrier, if present, for the water transfer reaction, will be expected to be considerably higher in ΔG°_{298}, mainly due to the unfavorable entropy associated with the bridged transition state for water transfer. Seeley et al. [25] found an activation energy for Eq. (38) of +2.7 kcal mol^{-1}.

$$Cl^-(H_2O) + CH_3Br \rightarrow Cl^-(CH_3Br) + H_2O \quad (38)$$

Correcting the calculated activation energy (+2.9 kcal mol^{-1}) for the non-solvated S_N2 reaction to match the experimental value of −1.8 kcal mol^{-1}, and applying this correction to the calculated activation energy for Eq. (38) gives a value of +2.5 kcal mol^{-1}. Even though the agreement is very close, the values cannot really be compared since they represent different processes. From the potential energy surface discussed below it can be seen that ligand switching is indeed energetically more favorable than the solvated S_N2 reaction.

The main question then is, are there, besides the solvated S_N2 reactions mentioned in the introduction, other systems possible for which true solvated S_N2 reactions can be observed? It does not seem unreasonable to assume that mono-solvated S_N2 reactions in the gas phase, if even these are possible to perform, are the closest one can get to the condensed phase counterparts. Obtaining such experimental

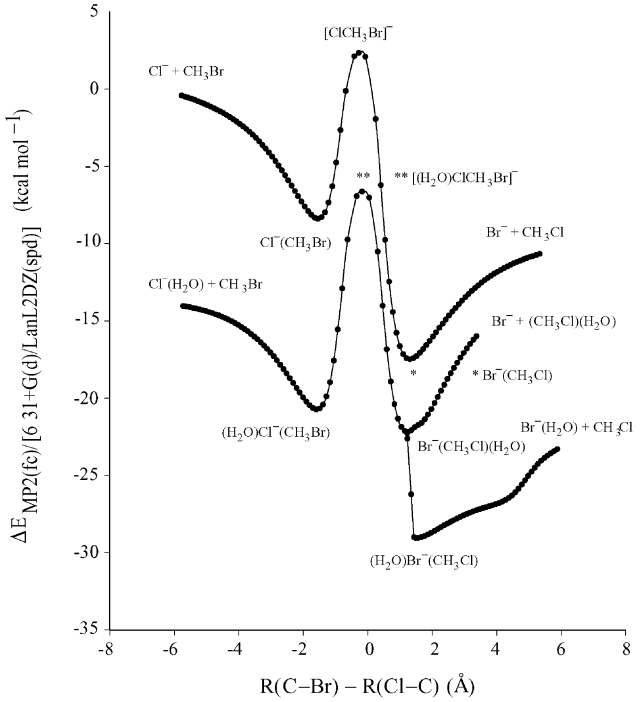

Fig. 8. MP2/[**c**/**d**] potential energy profiles for the $Cl^- + CH_3Br \rightarrow Br^- + CH_3Cl$ and $Cl^-(H_2O) + CH_3Br \rightarrow Br^- + (CH_3Cl)(H_2O)$ and $Br^-(H_2O) + CH_3Cl$ reactions.

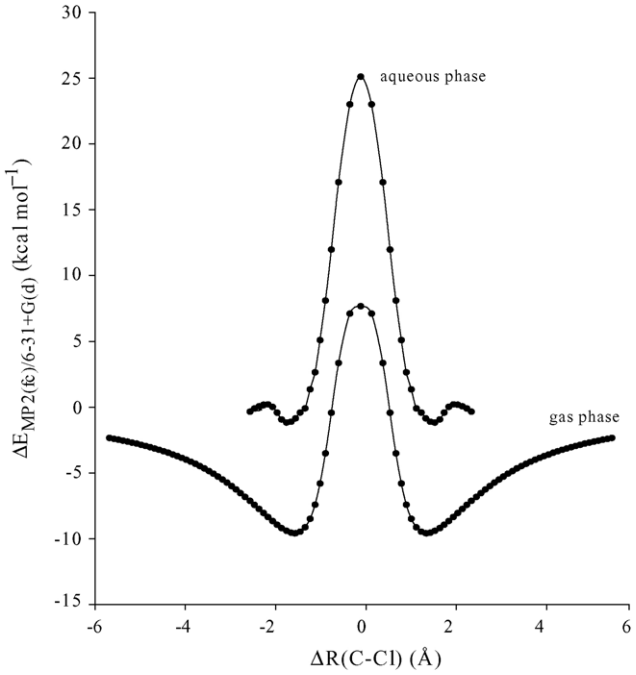

Fig. 9. MP2/**c** and MP2/**c** IPCM potential energy surface scan plots of the gas phase and water phase $Cl^- + CH_3Cl$ S_N2 reactions, respectively.

data is quite necessary to test the computational data, which can often be very method and/or system dependent. The reactivity of most larger clusters investigated to date show no S_N2 processes taking place. Producing less strongly bound clusters that could still show some reactivity seems unproductive since these do not relate well to the actual solution phase solvents used.

4.4. Potential energy surfaces

In Fig. 8 the results for potential energy surface scans for Eqs. (39)–(41) are shown.

$$Cl^- + CH_3Br \rightarrow Br^- + CH_3Cl \quad (39)$$

$$Cl^-(H_2O) + CH_3Br \rightarrow Br^- + (CH_3Cl)(H_2O) \quad (40)$$

$$Cl^-(H_2O) + CH_3Br \rightarrow Br^-(H_2O) + CH_3Cl \quad (41)$$

The reaction coordinate was taken to be the difference in the C–Br and C–Cl distances. For Eq. (39) the expected qualitative profile has been obtained, even though the barrier height relative to the reactants does not seem to agree with many experimental data or with various computational results that support the experimental data. For Eqs. (40) and (41), two different potential energy surfaces have been obtained, however this difference is only evident on the product side of the profile. For Eq. (40) the same reaction coordinate can be used like for Reaction 39. For Eq. (41) on the other hand, upon going from $Br^-(CH_3Cl)(H_2O)$ to $(H_2O)Br^-(CH_3Cl)$ an additional reaction coordinate for the water transfer should be taken into account. This transfer might simply be viewed as a rotation of the $Br^-(CH_3Cl)$ part of the complex. This would seem to be an accessible alternative to the symmetric bridge-like transition state that connects the $[(H_2O)ClCH_3Br]^{-\ddagger}$ and $[ClCH_3Br(H_2O)]^{-\ddagger}$ transition states. The expected increase in the transition state energy for the solvated S_N2 reaction is clearly observable. The occurrence of rotations in ion–molecule clusters to facilitate isomerization is not uncommon. For example, the unimolecular dissociation of the $Cl^-(HOCF_3)$ complex into $Cl^-(HF)$ and CF_2O has been shown to take place through a series of steps that include internal rotations in some of the intermediates (scheme (42)) [67].

$$\begin{aligned} Cl^-(HOCF_3) &\rightarrow [CF_3O^-(HCl)] \rightarrow {}^-OCF_3(HCl) \\ &\rightarrow Cl^-(HF)(CF_2O) \rightarrow (FH)Cl^-(CF_2O) \\ &\rightarrow Cl^-(HF) + CF_2O \end{aligned} \quad (42)$$

It does not seem unlikely, if the lifetime of the $Y^-(RX)(S)$ complex is sufficient and excess internal energy can be redistributed efficiently, for isomerization to the more stable $(S)Y^-(RX)$ complex to become possible, and consequently the relative amount of observable solvated product ions, $Y^-(S)$, may increase.

4.5. Gas phase mono-solvation versus condensed phase S_N2 reactions

In Fig. 9 the gas phase potential energy surface scan at the MP2/**c** level of theory for Eq. (43) is shown, together the

Table 13
Computational MP2 IPCM $\Delta E^{\ddagger}(\varepsilon)$ and $\Delta E(\varepsilon)$ values for the $Cl^-(S)_\infty + CH_3Cl(S)_\infty \rightarrow [ClCH_3Cl]^{-\ddagger}(S)_\infty$ and $Cl^-(CH_3Cl)(S)_\infty$ condensed phase S_N2 reactions for a variety of solvents

Solvent	ε	$\Delta E^{\#}(\varepsilon)$ (kcal mol^{-1})	$\Delta E(\varepsilon)$ (kcal mol^{-1})
Gas phase	1.00	+7.7	−9.6
Heptane	1.92	+16.0	
Benzene	2.247	+17.4	−4.6
Chloroform	4.9	+21.7	−2.6
THF	7.58	+22.5	−2.1
Acetone	20.7	+24.5	−1.4
Methanol	32.63	+24.8	
Acetonitrile	36.64	+24.8	
DMSO	46.7	+25.0	
Water	78.3	+25.1	−1.2

condensed phase analog in water (Eq. (44))

$$Cl^- + CH_3{}^*Cl \rightarrow {}^*Cl^- + CH_3Cl \quad (43)$$

$$Cl^-(H_2O)_\infty + CH_3{}^*Cl(H_2O)_\infty \rightarrow {}^*Cl^-(H_2O)_\infty + CH_3Cl(H_2O)_\infty \quad (44)$$

As expected, and as shown previously, the barrier in the condensed phase has increased dramatically, and the well-depths of the ion–molecule complexes have been reduced considerably [68–70]. In addition, there is a small barrier, corresponding to partial desolvation prior to formation of the ion–molecule complex. It was assumed that the transition state geometries in the gas and condensed phase are identical, and this was mainly done for CPU time saving purposes. The results for the various MP2/**c** IPCM barrier heights and well-depths, $\Delta E^{\ddagger}(\varepsilon)$ and $\Delta E(\varepsilon)$, respectively, in a variety of solvents spanning a large range of dielectric constants, ε, are shown in Table 13. The results are plotted in Figs. 10 and 11. It can be seen that in going from the gas phase to THF as solvent, a large increase in $\Delta E^{\ddagger}(\varepsilon)$ is observed, while upon going from acetone to water it levels off. A similar but inverse trend is observed by plotting ε versus $-\Delta E(\varepsilon)$, with a large drop going from the gas phase to THF, while from acetone to water it levels off. Plotting $-\Delta E(\varepsilon)$ versus $\Delta E^{\#}(\varepsilon)$ gives a nearly linear correlation (Fig. 12). To see how well the chosen method actually performs, computations on various other condensed phase systems were performed for which experimental activation energies are known. The results in Table 14 show that good to excellent agreement can be obtained except for systems where F^- is the nucleophile. The experimental results for the $Cl^- + CH_3Br$ and $Br^- + CH_3Br$ reactions may be inaccurate, as discussed by Moelwyn-Hughes and co-workers [2–4]. As noted above, the results for most experiments in Table 1 show that even the addition of one solvent molecule will dramatically slow the reaction compared to the non-solvated gas phase reaction by almost two orders of magnitude. It would be interesting to see if for mono-solvated S_N2 reactions the linear correlation from Fig. 12 also applies. In Fig. 13 a plot of $-\Delta H^{\circ}_{298}$ versus $\Delta H^{\ddagger}_{298}$, both from MP2/**b**//MP2/**a** computations for Eqs. (45) and (46),

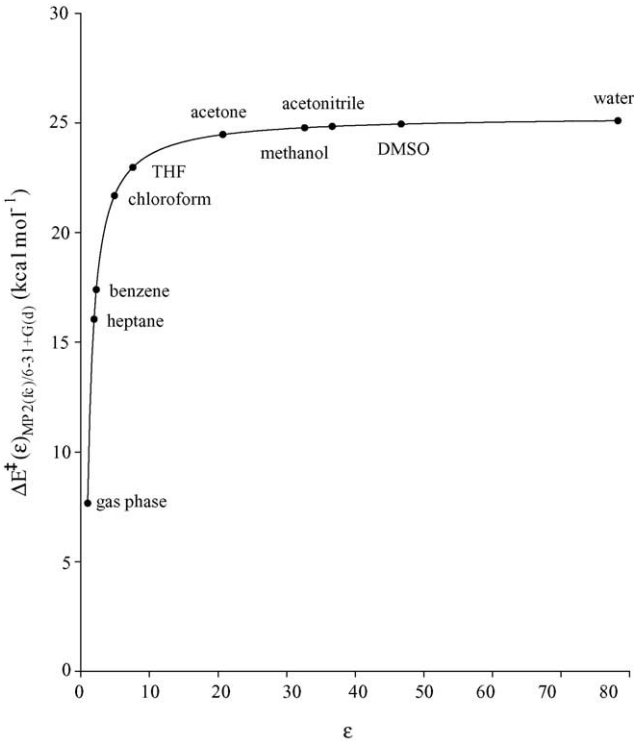

Fig. 10. Plot of the dielectric constant (ε) vs. the MP2/**c** activation energy for the $Cl^- + CH_3Cl$ S_N2 reaction, $\Delta E^{\ddagger}(\varepsilon)_{MP2(fc)/6\text{-}31+G(d)}$, in various solvents.

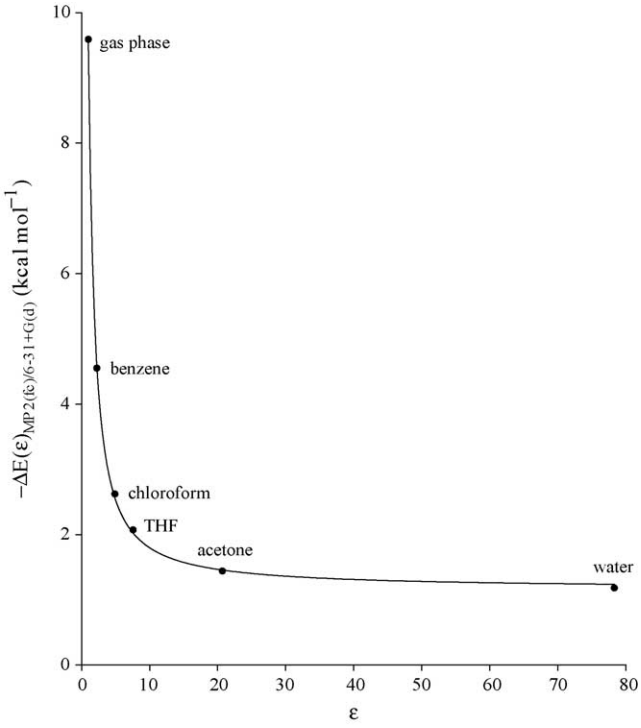

Fig. 11. Plot of the dielectric constant (ε) vs. the negative MP2/**c** complexation energy for the $Cl^- + CH_3Cl$ S_N2 reaction, $-\Delta E(\varepsilon)_{MP2(fc)/6\text{-}31+G(d)}$, in various solvents.

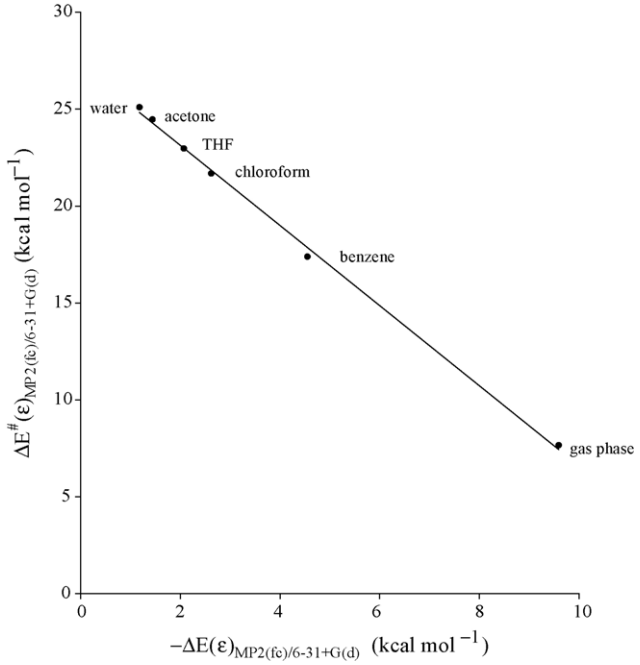

Fig. 12. Plot of $-\Delta E(\varepsilon)_{MP2(fc)/6\text{-}31+G(d)}$ vs. $\Delta E^{\ddagger}(\varepsilon)_{MP2(fc)/6\text{-}31+G(d)}$ for the $Cl^- + CH_3Cl$ S_N2 reaction in various solvents.

respectively, is shown (S = H_2O, H_2S, NH_3, PH_3)

$$Cl^-(S) + CH_3Cl \rightleftharpoons (S)Cl^-(CH_3Cl) \quad (45)$$

$$Cl^-(S) + CH_3Cl \rightarrow [(S)ClCH_3Cl]^- \quad (46)$$

In Fig. 14 a plot of $-\Delta H^{\circ}$ for Eq. (47), from PHPMS results of this work, versus $\Delta E^{\ddagger}$ for Eq. (48), from Mohamed and Jensen [33], is shown (S = CH_3OH, CH_3CN, $(CH_3)_2CO$).

$$Cl^-(S) + (CH_3)_2CHCl \rightleftharpoons (S)Cl^-((CH_3)_2CHCl) \quad (47)$$

$$Cl^-(S) + (CH_3)_2CHCl \rightarrow [(S)ClCH(CH_3)_2Cl]^- \quad (48)$$

The $\Delta E^{\ddagger}$ values were obtained as follows: $\Delta E^{\ddagger}$ values for $[ClRCl]^-$ (R = Me, Et, *i*-Pr, *t*-Bu) were taken as averages from B3LYP/**c** and MP2/**c**//B3LYP/**c** computations,

Table 14
Computational MP2 IPCM $\Delta E^{\ddagger}$ and experimental E_a values for $X^-(S)_\infty + CH_3Y(S)_\infty \rightarrow [XCH_3Y]^{-\ddagger}(S)_\infty$ (X, Y = F, Cl, Br, I; S = H_2O, $(CH_3)_2CO$) condensed phase S_N2 reactions

X^-	CH_3Y	Solvent	$\Delta E^{\#}$ (kcal mol^{-1})	E_a (kcal mol^{-1})	Reference
Cl^-	CH_3I	Acetone	+17.0	+16.5	[2]
I^-	CH_3Cl	Acetone	+18.1	+18.0	[2]
Cl^-	CH_3Br	Acetone	+20.6	+15.7	[84]
Br^-	CH_3Br	Acetone	+19.4	+15.8	[85]
F^-	CH_3Cl	Water	+14.9	+26.9	[3]
F^-	CH_3Br	Water	+14.2	+25.2	[3]
F^-	CH_3I	Water	+11.4	+25.2	[3]
Cl^-	CH_3Br	Water	+21.2	+24.6	[3]
Br^-	CH_3Br	Water	+20.0	+23.7	[9]
I^-	CH_3F	Water	+25.1	+23.1	[3]

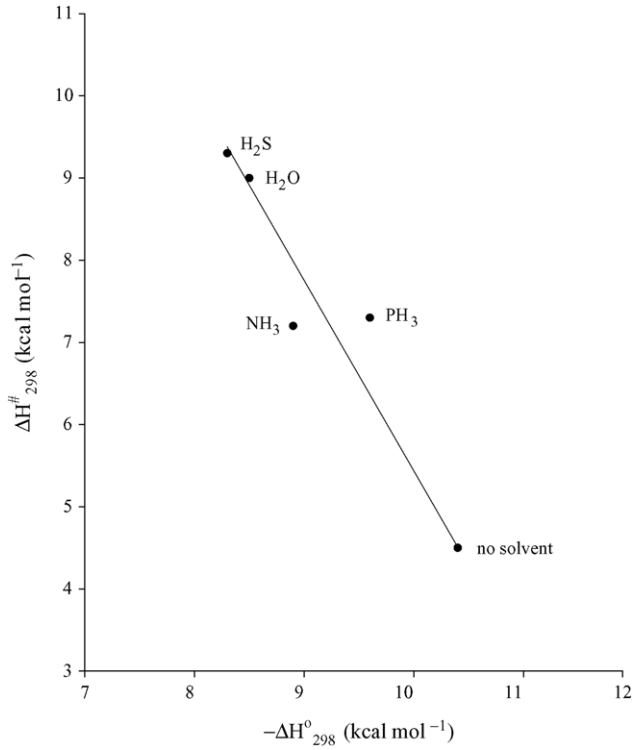

Fig. 13. Plot of the MP2/**b**//MP2/**a** $-\Delta H^{\circ}_{298}$ vs. $-\Delta H^{\ddagger}_{298}$ results for the $Cl^-(S) + CH_3Cl$ mono-solvated S_N2 reaction.

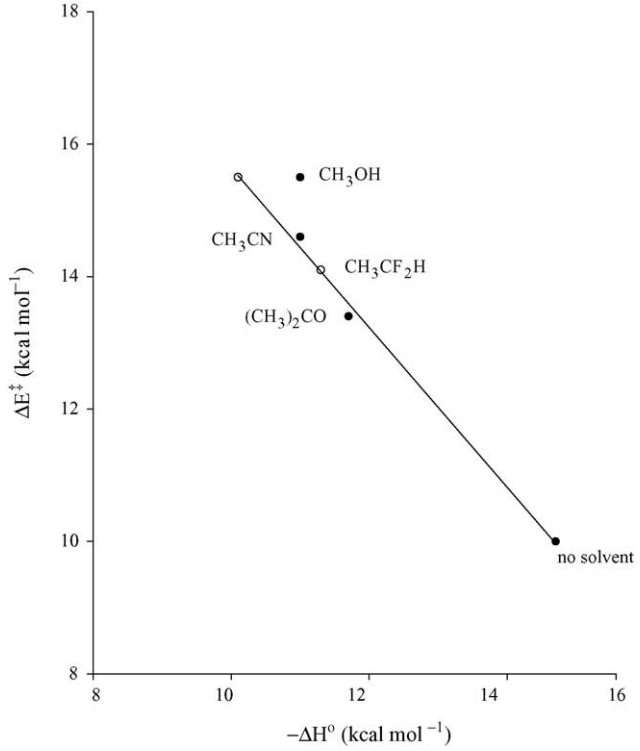

Fig. 14. Plot of the PHPMS $-\Delta H^{\circ}$ vs. the calculated $\Delta E^{\ddagger}$ results for the $Cl^-(S) + (CH_3)_2CHCl$ mono-solvated S_N2 reactions.

and these values (3.5, 7.2, 10.0, and 17.4 kcal mol^{-1}, respectively). The $\Delta E^{\ddagger}$ values for $[(S)ClCH_3Cl]^-$ were estimated by taking the B3LYP/**c** $\Delta E^{\ddagger}$ values and adding 5.0 kcal mol^{-1}, a value based on the average of the $\Delta E^{\ddagger}$ values for $[(H_2O)ClRCl]^-$. This gives $\Delta E^{\ddagger}$ values for S = CH_3OH, CH_3CN, and $(CH_3)_2CO$ of 15.5, 14.6, and 13.4 kcal mol^{-1}, respectively. It seems that the ΔH° value for S = CH_3OH should be around −10.1 kcal mol^{-1}. In addition, for S = CH_3CF_2H a $\Delta E^{\ddagger}$ value of 14.1 kcal mol^{-1} can be estimated from interpolation of the fitted line. The latter two values are indicated by white dots in Fig. 14. In Fig. 13 the results for S = NH_3 and PH_3 are somewhat off the line, but the overall result and conclusion do not change. These results seem to indicate that from a thermochemical point of view, mono-solvated S_N2 reactions in the gas phase already show features of their condensed phase counterparts.

5. Conclusion

In this work various aspects of the structures and thermochemistry of solvated S_N2 complexes and transition states have been investigated using both experimental, PHPMS and ab initio computational methods.

The structures of solvated S_N2 complexes, $(S)X^-(CH_3Y)$, and transition states, $[(S)XCH_3Y]^{-\ddagger}$, can show very different bonding characteristics from those of the halide ion–solvent, $X^-(S)$, and S_N2 complexes, $X^-(CH_3Y)$, depending upon the solvent.

The experimental thermochemistry shows minor solvent effects. The two different equilibria, solvation of a S_N2 complexes and a solvated S_N2 reaction, have different thermochemistry, and can be understood in terms of a thermochemical cycle. Most data present are completely new, and may provide a base to test theoretical models on these systems.

The MP2/**b**//MP2/**a** and G2(MP2) computations provide close agreement with experimental thermochemical data for the formation of $X^-(S)$ complexes. The ΔH°_{298} values for the formation of the investigated $(S)X^-(CH_3Cl)$ complexes seem to be reasonable, as opposed to the ΔS°_{298} values. For both the non-solvated and solvated S_N2 transition states investigated, $[XCH_3Y]^{-\ddagger}$ and $[(S)XCH_3Y]^{-\ddagger}$, respectively, the MP2/**b**//MP2/**a** computations seem to overestimate $\Delta H^{\ddagger}_{298}$.

Linear correlations between ΔH°_{298} for the formation of $Cl^-(S)$ (S = H_2O, H_2S, NH_3, PH_3, SO_2), and ΔH°_{298} and $\Delta H^{\ddagger}_{298}$ for the formation of $(S)Cl^-(CH_3Cl)$ and $[(S)ClCH_3Cl]^{-\ddagger}$, respectively have been found, except for $\Delta H^{\ddagger}_{298}$ with S = SO_2).

To date only a few systems have shown real solvated S_N2 reactivity, most notably, the $F^-(ROH) + CH_3X$ reactions (R = H, alkyl; X = Br, I). Other systems without solvated fluoride ion should be possible and seem more practical and interesting.

The potential energy profiles for the solvated S_N2 reaction between $Cl^-(H_2O)$ and CH_3Br, calculated at the MP2/[**c**/**d**] level of theory, show that formation of Br^- and $Br^-(H_2O)$ proceeds through two different profiles. Isomerization from $Br^-(CH_3Cl)(H_2O)$ to $(H_2O)Br^-(CH_3Cl)$ can be accomplished by a rotation of the $Br^-(CH_3Cl)$ part. This process is energetically favorable and leads to a net solvent transfer.

For the condensed phase $Cl^- + CH_3Cl$ S_N2 reactions in a variety of solvents, the MP2/**c** IPCM $-\Delta E(\varepsilon)$ and $\Delta E^{\ddagger}(\varepsilon)$ values show a leveling off as the dielectric constant increases to around 20 (acetone). Plotting $-\Delta E(\varepsilon)$ versus $\Delta E^{\ddagger}(\varepsilon)$ gives a linear correlation, and similar behavior is observed for the MP2/**b**//MP2/**a** computations of the $Cl^-(S) + CH_3Cl$ reactions (S = H_2O, H_2S, NH_3, PH_3, SO_2), and PHPMS results and computations from Mohamed and Jensen for the $Cl^-(S) + (CH_3)_2CHCl$ reactions (S = CH_3OH, CH_3CN, $(CH_3)_2CO$). This may indicate that, in addition to dramatic changes in the kinetics upon mono-solvation, the thermochemistry may also begin to adopt condensed phase features.

Acknowledgements

The authors would like to thank the Natural Sciences and Engineering Research Council of Canada (NSERC) and the donors of the Petroleum Research Fund, administered by the American Chemical Society, for financial support. Dr. Y. Okuno is thanked for providing help with the solvated transition state computations.

References

[1] C.K. Ingold, Structure and Reactivity in Organic Chemistry, 2nd ed., Cornell University Press, Ithaca, NY, 1969, and references cited therein.
[2] F. Aziz, E.A. Moelwyn-Hughes, J. Chem. Soc. (1959) 2635.
[3] B.W. Marshall, E.A. Moelwyn-Hughes, J. Chem. Soc. (1959) 2640.
[4] R.H. Bathgate, E.A. Moelwyn-Hughes, J. Chem. Soc. (1959) 2642.
[5] R. Alexander, E.C.F. Ko, A.J. Parker, T.J. Broxton, J. Am. Chem. Soc. 90 (1968) 5049, and references cited therein.
[6] A.J. Parker, Chem. Rev. 69 (1969) 1, and references cited therein.
[7] S.R. Hartshorn, Aliphatic Nucleophilic Substitution, Cambridge University Press, London, 1973.
[8] A. Streitweiser Jr., Solvolytic Displacement Reactions, McGraw-Hill, New York, NY, 1973.
[9] W.J. Albery, M.M. Kreevoy, Adv. Phys. Org. Chem. 16 (1978) 87, and references cited therein.
[10] S.S. Shaik, H.B. Schlegel, S. Wolfe, Theoretical Aspects of Physical Organic Chemistry. The S_N2 Mechanism, Wiley, New York, NY, 1992, and references cited therein.
[11] D.K. Bohme, G.I. Mackay, J. Am. Chem. Soc. 103 (1981) 978.
[12] M. Henchman, J.F. Paulson, P.M. Hierl, J. Am. Chem. Soc. 105 (1983) 5509.
[13] M. Henchman, P.M. Hierl, J.F. Paulson, J. Am. Chem. Soc. 107 (1985) 2812.
[14] D.K. Bohme, A.B. Raksit, J. Am. Chem. Soc. 106 (1984) 3447.
[15] D.K. Bohme, A.B. Raksit, Can. J. Chem. 63 (1985) 3007.
[16] P.M. Hierl, A.F. Ahrens, M. Henchman, A.A. Viggiano, J.F. Paulson, D.C. Clary, J. Am. Chem. Soc. 108 (1986) 3142.

[17] P.M. Hierl, A.F. Ahrens, M. Henchman, A.A. Viggiano, J.F. Paulson, Int. J. Mass Spectrom. Ion Processes 81 (1987) 101.
[18] P.M. Hierl, A.F. Ahrens, M.J. Henchman, A.A. Viggiano, J.F. Paulson, Faraday Discuss. Chem. Soc. 85 (1988) 37.
[19] K. Giles, E.P. Grimsrud, J. Phys. Chem. 97 (1993) 1318.
[20] R.A.J. O'Hair, G.E. Davico, J. Hacaloglu, T.T. Dang, C.H. DePuy, V.M. Bierbaum, J. Am. Chem. Soc. 116 (1994) 3609.
[21] P.M. Hierl, J.F. Paulson, M.J. Henchman, J. Phys. Chem. 99 (1995) 15655.
[22] A.A. Viggiano, S.T. Arnold, R.A. Morris, A.F. Ahrens, P.M. Hierl, J. Phys. Chem. 100 (1996) 14397.
[23] S.L. Craig, J.I. Brauman, J. Am. Chem. Soc. 118 (1996) 6786.
[24] J.V. Seeley, R.A. Morris, A.A. Viggiano, J. Phys. Chem. A 101 (1997) 4598.
[25] J.V. Seeley, R.A. Morris, A.A. Viggiano, H. Wang, W.L. Hase, J. Am. Chem. Soc. 119 (1997) 577.
[26] S.L. Craig, J.I. Brauman, J. Am. Chem. Soc. 121 (1999) 6690.
[27] K. Morokuma, J. Am. Chem. Soc. 104 (1982) 3732.
[28] W.-P. Hu, D.G. Truhlar, J. Am. Chem. Soc. 116 (1994) 7797.
[29] F.M. Bickelhaupt, E.J. Baerends, N.M.M. Nibbering, Chem. Eur. J. 2 (1996) 196.
[30] H. Tachikawa, J. Phys. Chem. A 104 (2000) 497.
[31] H. Tachikawa, J. Phys. Chem. A 105 (2001) 1260.
[32] S. Raugei, G. Cardini, V. Schettino, J. Chem. Phys. 114 (2001) 4089.
[33] A.A. Mohamed, F. Jensen, J. Phys. Chem. A 105 (2001) 3259.
[34] S.C. Tucker, D.G. Truhlar, J. Am. Chem. Soc. 112 (1990) 3347.
[35] X.G. Zhao, S.C. Tucker, D.G. Truhlar, J. Am. Chem. Soc. 113 (1991) 826.
[36] X.G. Zhao, D.-H. Lu, Y.-P. Liu, G.C. Lynch, D.G. Truhlar, J. Chem. Phys. 97 (1992) 6369.
[37] M. Re, D. Laria, J. Chem. Phys. 105 (1996) 4584.
[38] Y. Okuno, J. Chem. Phys. 105 (1996) 5817.
[39] Y. Okuno, J. Am. Chem. Soc. 122 (2000) 2925.
[40] J.E. Szulejko, J.J. Fisher, T.B. McMahon, J. Wronka, Int. J. Mass Spectrom. Ion Processes 83 (1988) 147.
[41] M.J. Frisch, G.W. Trucks, H.B. Schlegel, G.E. Scuseria, M.A. Robb, J.R. Cheeseman, V.G. Zakrzewski, J.A. Montgomery Jr., R.E. Stratmann, J.C. Burant, S. Dapprich, J.M. Millam, A.D. Daniels, K.N. Kudin, M.C. Strain, O. Farkas, J. Tomasi, V. Barone, M. Cossi, R. Cammi, B. Mennucci, C. Pomelli, C. Adamo, S. Clifford, J. Ochterski, G.A. Petersson, P.Y. Ayala, Q. Cui, K. Morokuma, D.K. Malick, A.D. Rabuck, K. Raghavachari, J.B. Foresman, J. Cioslowski, J.V. Ortiz, A.G. Baboul, B.B. Stefanov, G. Liu, A. Liashenko, P. Piskorz, I. Komaromi, R. Gomperts, R.L. Martin, D.J. Fox, T. Keith, M.A. Al-Laham, C.Y. Peng, A. Nanayakkara, C. Gonzalez, M. Challacombe, M.W. Gill, B. Johnson, W. Chen, M.W. Wong, J.L. Andres, C. Gonzalez, M. Head-Gordon, E.S. Replogle, J.A. Pople, Gaussian 98, Gaussian Inc, Pittsburgh, PA, 1998, Revision A.7.
[42] C.C.J. Roothan, Rev. Mod. Phys. 23 (1951) 69.
[43] C. Møller, M.S. Plesset, Phys. Rev. 46 (1934) 618.
[44] W.J. Hehre, R. Ditchfield, J.A. Pople, J. Chem. Phys. 56 (1972) 2257.
[45] M.M. Francl, W.J. Petro, W.J. Hehre, J.S. Binkley, M.S. Gordon, D.J. DeFrees, J.A. Pople, J. Chem. Phys. 77 (1982) 3654.
[46] T. Clark, J. Chandrasekhar, P.V.R. Schleyer, J. Comp. Chem. 4 (1983) 294.
[47] R. Krishnam, J.S. Binkley, R. Seeger, J.A. Pople, J. Chem. Phys. 72 (1980) 650.
[48] P.M.W. Gill, B.G. Johnson, J.A. Pople, M.J. Frisch, Chem. Phys. Lett. 97 (1992) 499.
[49] A.P. Scott, L. Radom, J. Phys. Chem. 100 (1996) 16502.
[50] From a least-squares fit of unscaled HF/6-31+G(d,p) normal mode vibrational frequencies of CH_3Cl, H_2O, H_2S, NH_3, PH_3, and SO_2 versus experimental frequencies from reference 51.
[51] T. Shimanouchi, Tables of Molecular Vibrational Frequencies Consolidated Volume I, National Bureau of Standards, Washington, DC, 1972, p. 1.
[52] M.J. Frisch, J.A. Pople, J.S. Binkley, J. Chem. Phys. 80 (1984) 3265.
[53] P.C. Hariharan, J.A. Pople, Theor. Chim. Acta 28 (1973) 213.
[54] P.J. Hay, W.R. Wadt, J. Chem. Phys. 82 (1985) 284.
[55] M.N. Glukhovtsev, A. Pross, M.P. McGrath, L. Radom, J. Chem. Phys. 103 (1995) 1878.
[56] L.A. Curtiss, K. Raghavachari, J.A. Pople, J. Chem. Phys. 94 (1993) 7221.
[57] Gaussian 98 User's Reference, second ed., Gaussian Inc., 1999.
[58] J.B. Foresman, T.A. Keith, K.B. Wiberg, J. Snoonian, M.J. Frisch, J. Phys. Chem. 100 (1996) 16098.
[59] D.R. Lide (Ed.), CRC Handbook of Chemistry and Physics, Ref. Data, 76th ed., Boca Raton, FL, CRC, 1995.
[60] L. Deng, V. Branchadell, T. Ziegler, J. Am. Chem. Soc. 116 (1994) 10645, and references cited therein.
[61] M.N. Glukhovtsev, A. Pross, L. Radom, J. Am. Chem. Soc. 117 (1995) 2024, and references cited therein.
[62] M.N. Glukhovtsev, R.D. Bach, A. Pross, L. Radom, Chem. Phys. Lett. 260 (1996) 558.
[63] M.N. Glukhovtsev, A. Pross, L. Radom, J. Am. Chem. Soc. 118 (1996) 6273, and references cited therein.
[64] S. Parthiban, G. de Oliveira, J.M.L. Martin, J. Phys. Chem. A 105 (2001) 895, and references cited therein.
[65] C. Li, P. Ross, J.E. Szulejko, T.B. McMahon, J. Am. Chem. Soc. 118 (1996) 9360.
[66] http://webbook.nist.gov/chemistry/.
[67] B. Bogdanov, Ph.D. Thesis, University of Waterloo, 2001.
[68] J. Chandrassekhar, S.F. Smith, W.L. Jorgensen, J. Am. Chem. Soc. 106 (1984) 3049.
[69] J. Chandrassekhar, S.F. Smith, W.L. Jorgensen, J. Am. Chem. Soc. 107 (1985) 154.
[70] J. Chandrassekhar, W.L. Jorgensen, J. Am. Chem. Soc. 107 (1985) 2974.
[71] B. Bogdanov, M. Peschke, D.S. Tonner, J.E. Szulejko, T.B. McMahon, Int. J. Mass Spectrom. 185–187 (1999) 707.
[72] K. Hiraoka, S. Mizuse, S. Yamabe, J. Phys. Chem. 92 (1988) 3943.
[73] D.H. Evans, R.G. Keesee, A.W. Castleman Jr., J. Chem. Phys. 86 (1987) 2927.
[74] B. Bogdanov, H.J.S. Lee, T.B. McMahon, Int. J. Mass Spectrom. 210–211 (2001) 387.
[75] R.C. Dougherty, J. Dalton, J.D. Roberts, Org. Mass Spectrom. 8 (1974) 77.
[76] R.C. Dougherty, J.D. Roberts, Org. Mass Spectrom. 8 (1974) 81.
[77] S.E. Barlow, J.M. Van Doren, V.M. Bierbaum, J. Am. Chem. Soc. 110 (1988) 7240.
[78] S.C. Tucker, D.G. Truhlar, J. Am. Chem. Soc. 112 (1990) 3338.
[79] B.D. Wladkowski, J.I. Brauman, J. Phys. Chem. 97 (1993) 13158.
[80] S.T. Graul, M.T. Bowers, J. Am. Chem. Soc. 116 (1994) 3875.
[81] G. Caldwell, T.F. Magnera, P. Kebarle, J. Am. Chem. Soc. 106 (1984) 959.
[82] W.B. Knighton, J.A. Bognar, P.M. O'Connor, E.P. Grimsrud, J. Am. Chem. Soc. 115 (1993) 22079.
[83] W.-P. Hu, D.G. Truhlar, J. Am. Chem. Soc. 117 (1995) 10726.
[84] E.D. Hughes, C.K. Ingold, J.D.H. Mackie, J. Chem. Soc. (1954) 3173.
[85] P.B.D. de la Mare, J. Chem. Soc. (1954) 3180.